

Constraining DM properties with SPI

Alexey Boyarsky^{1*}, Denys Malyshev^{2,3}, Andrey Neronov^{4*}, Oleg Ruchayskiy⁵

¹ CERN, PH/TH, CH-1211 Geneve 23, Switzerland

² Bogolyubov Institute for Theoretical Physics, Kiev, 03780, Ukraine

³ Dublin Institute for Advanced Studies, 31 Fitzwilliam Place, Dublin 2, Ireland

⁴ INTEGRAL Science Data Center, Chemin d'Écogia 16, 1290 Versoix, Switzerland
Geneva Observatory, 51 ch. des Maillettes, CH-1290 Sauverny, Switzerland

⁵ École Polytechnique Fédérale de Lausanne, Institute of Theoretical Physics,
FSB/ITP/LPPC, BSP 720, CH-1015, Lausanne, Switzerland

ABSTRACT

We search for a spectral line produced by a dark matter (DM) particle with the mass in the range $40 \text{ keV} < M_{\text{DM}} < 14 \text{ MeV}$, decaying in the DM halo of the Milky Way, using a high-resolution spectrometer SPI on board of *INTEGRAL* satellite. To distinguish the DM decay line from numerous instrumental lines, found in the SPI background spectrum, we study the dependence of the intensity of the line signal on the offset of the SPI pointing from the direction toward the Galactic Center (GC). After a critical analysis of the uncertainties of the DM density profile in the inner Galaxy we find that the intensity of the DM decay line should decrease by at least a factor of 3 when the offset from GC increases from 0° to 180° . We find that such a pronounced variation of the line flux across the sky is not observed for any line, detected with the significance higher than 3σ in the SPI background spectrum. Possible DM decay origin is not ruled out only for the unidentified spectral lines, having low ($\sim 3\sigma$) significance or coinciding in position with the instrumental ones. In the energy interval $20 \text{ keV} - 7 \text{ MeV}$ we derive restrictions on the DM decay line flux, implied by the (non)detection of the DM decay line. For a particular DM candidate, the sterile neutrino of mass M_{DM} , we derive a bound on the mixing angle.

Key words: Cosmology – dark matter; Galaxy – halo; techniques – spectroscopic; methods – data analysis

1 INTRODUCTION

Dark matter in the Universe

There exists a vast body of evidence, suggesting that the large fraction of matter in the Universe exists in the form of the *Dark matter (DM)*. However, while the total density of the DM is measured with a very high precision ($\Omega_{\text{DM}} h^2 = 0.105_{-0.009}^{+0.007}$, Spergel et al. 2007), little is known about its properties apart from that. The possibility that the DM is composed of the Standard Model (SM) particles has been ruled out for a long time already. Indeed, the DM cannot be made out of baryons, as producing such an amount of baryonic matter would require drastic modifications of the scenario of the Big Bang nucleosynthesis (BBN), otherwise successfully describing the abundances of light elements (see e.g. Dar 1995). Recent microlensing experiments rule out the possibility

that another type of baryonic DM – MACHOs (massive compact halo objects) – constitute dominant fraction of mass in the halo (Alcock et al. 2000; Lasserre et al. 2000; Alard 1999). The only non-baryonic DM candidate in the SM candidates – (left-handed) neutrino – is ruled out from the large scale structure (LSS) considerations (see e.g. Bond et al. 1980; Hannestad & Raffelt 2004; Crotty et al. 2004).

What are the properties of a successful DM candidate? First of all, this particle should be massive. Many extensions of the SM present the DM candidates with the masses ranging from $\sim 10^{-10} \text{ eV}$ (massive gravitons, Dubovsky et al. 2005) and $\sim 10^{-6} \text{ eV}$ (axions) to hundreds of GeV (WIMPs) and even to 10^{13} GeV (WIMPZILLA, Kuzmin & Tkachev 1998, 1999; Chung et al. 1999). For a review of particle physics DM candidates see e.g. Bergstrom (2000); Bertone et al. (2005); Carr et al. (2006).

Secondly, there should exist mechanisms of DM production with the correct abundances. The production mechanism in particular determines the velocity distribution of particles in the early Universe. This velocity distribution can, in principle, be probed exper-

* On leave of absence from Bogolyubov Institute for Theoretical Physics, Kiev, Ukraine

imentally. Namely, if during the structure formation epoch the DM particles had non-negligible velocities, they would “erase” density fluctuations at scales, smaller than their *free-streaming length*. To differentiate various models in accordance with this property, the DM candidates with the negligible velocity dispersion (and, correspondingly, free-streaming) are called *cold* DM (CDM), while those with the free-streaming of the order of ~ 1 Mpc are considered to be *warm* (WDM).¹ It is possible to constrain the free-streaming length of a particular DM candidate by probing the structure of the Universe at galaxy-size scales. This can be done through the analysis of the Lyman- α forest data (Hui et al. 1997). Lyman- α analysis puts an upper bound on the free-streaming of the DM particles (Hansen et al. 2002; Viel et al. 2005; Seljak et al. 2006; Viel et al. 2006; Viel et al. 2007). It should be noted however that currently existing interpretation of the Lyman- α data is model-dependent, as, apart from a number of astrophysical assumptions (see Hui et al. 1997) and complicated hydrodynamic simulations, it relies on *a priori* assumptions about the velocity distribution of the DM particles.

Another way to differentiate between CDM and WDM models is to compare the N-body numerical simulations of the DM distribution in the Milky Way-type halo with the actual observations. The observations point out at the existence of the smallest scale at which the DM exists (Gilmore et al. 2006, 2007; Gilmore 2007; Koposov et al. 2007). These results seem to show the discrepancy with the N-body simulations in CDM models (see e.g. Moore 1994; Moore et al. 1999; Klypin et al. 1999; Bode et al. 2001; Avila-Reese et al. 2001; Goerdt et al. 2006) and to prefer DM model with non-zero free streaming at the galactic scale. On the other hand, the numerical simulations were performed only in the simplest cases and, for example, do not take into account baryons. Therefore it is too early to say what are the final predictions of different types of models and whether CDM or WDM models are really preferred (see also Simon & Geha (2007); Penarrubia et al. (2007)).

Usually it is also required that the DM candidate is stable. For the most popular DM candidate – weakly interacting massive particles (WIMPs), this is related to the fact that the particles of \sim electroweak mass, having weak strength interaction with SM matter (required to produce the correct amount of DM), would decay too fast and would not be “dark”. If, however, the DM particle interacts with the SM much weaker than WIMPs, it can well have a finite (although cosmologically long) life time.

There exist several unstable (decaying) DM candidates e.g. gravitino (Baltz & Murayama 2003; Cembranos et al. 2006). In this paper we will concentrate mainly on one candidate – sterile neutrino – (although our results will be applicable for any type of decaying DM). Constraints on the decaying DM were analyzed in de Rujula & Glashow (1980); Berezhiani et al. (1987); Doroshkevich et al. (1989); Berezhiani et al. (1990); Berezhiani & Khlopov (1990); Bertone et al. (2007); Zhang et al. (2007) (see also the book by Khlopov 1997).

Sterile neutrino DM

It was noticed long ago that the right-handed (or as it is often called *sterile*) neutrino with the mass in the keV range would represent a viable DM candidate (Dodelson & Widrow 1994). Such

¹ The left-handed neutrino would represent *hot* DM in this terminology, i.e. the DM with the free-streaming length $\gg 1$ Mpc.

a neutrino would interact with the rest of the matter only via the quadratic mixing with left-handed (*active*) neutrinos and therefore (although not stable) could have cosmologically long life-time. At the same time, it could be produced in the early Universe with the correct abundances (Dodelson & Widrow 1994; Shi & Fuller 1999; Shaposhnikov & Tkachev 2006). One of the decay channels of the unstable sterile neutrinos includes emission of photons of the energy equal to half of the sterile neutrino rest energy. This potentially provides a possibility to observe the decays of DM sterile neutrinos via detection of a characteristic spectral line in the spectra of astrophysical objects with large DM concentration.

Recently this DM candidate attracted a lot of attention (see e.g. Shaposhnikov (2007) and references therein). It was found that a very modest and natural extension of the SM by 3 right-handed neutrinos (making the SM more symmetric as all SM fermions, including neutrino, would have now their left and right handed counterparts) provides viable extension of the theory, capable of solving several “beyond the SM” problems. First of all, such an extension makes neutrinos massive and thus provides maybe the simplest and the most natural explanation of the phenomenon of “neutrino oscillations” (see e.g. Fogli et al. (2006); Strumia & Vissani (2006); Giunti (2007) for reviews). The smallness of neutrino masses in this model (called ν MSM in Asaka & Shaposhnikov 2005) is achieved via the usual see-saw mechanism with Majorana masses of right-handed neutrinos being below electroweak scale.²

Secondly, if two heavier sterile neutrinos (N_2 and N_3) are almost degenerate in mass and have their masses between $\mathcal{O}(100)$ MeV and $\mathcal{O}(20)$ GeV, the ν MSM provides the mechanism of generating the baryon asymmetry of the Universe. Thirdly, the lightest sterile neutrino N_1 can have arbitrary mass and arbitrarily weak coupling with the (active) neutrino sector. At the same time, it can be produced in the early Universe in the correct amounts. It represents therefore the DM particle in the ν MSM. Thus, altogether the ν MSM represents (arguably) the simplest extension of the SM, capable of explaining three important questions: origin and smallness of neutrino masses, baryon asymmetry in the Universe and the existence of the DM.

Existing restrictions on sterile neutrino DM parameters.

What are the current restrictions on parameters (mass and *mixing*) of sterile neutrino DM? First of all, as any fermionic DM, sterile neutrino’s mass should satisfy the the universal Tremaine-Gunn lower bound (Tremaine & Gunn 1979; Dalcanton & Hogan 2001): $M_{\text{DM}} \gtrsim 300 - 500$ eV.³

Next, as the sterile neutrino possesses the (two-body) radiative decay channel: $N_1 \rightarrow \nu + \gamma$, the emitted photon would carry the energy $E_\gamma = M_{\text{DM}}/2$. A large flux of such photons is expected from the large concentrations of the DM sterile neutrinos, like galaxies or galaxy clusters.

Recently an extensive search of the DM decay line in the region of masses $M_{\text{DM}} \lesssim 20$ keV was conducted, using the data of *Chandra* (Riemer-Sørensen et al. 2006; Boyarsky et al.

² The fact that the ν MSM does not introduce any new scale above the electroweak one, makes this theory especially appealing from the point of view of its experimental verification/falsification.

³ A stronger lower bound from Ly- α (Seljak et al. 2006; Viel et al. 2006; Viel et al. 2007) can be obtained in the case of the particular production mechanisms – the Dodelson-Widrow scenario (Dodelson & Widrow 1994). For other possible production mechanisms (e.g. Shi & Fuller 1999; Shaposhnikov & Tkachev 2006) the Ly- α constraints should be reanalyzed.

2006d; Abazajian et al. 2007) and *XMM-Newton* (Boyarsky et al. 2006a,b,c; Watson et al. 2006; Boyarsky et al. 2007a). The region of soft X-ray (down to energies 0.2 keV) was explored by Boyarsky et al. (2007b) with the use of the wide field of view spectrometer (McCammon et al. 2002). The non-observation of the DM decay line in X-ray, combined with the first principles calculation of DM production in the early Universe (Asaka et al. 2007), implies that the Dodelson & Widrow (1994) (DW) scenario can work only if the sterile neutrino mass is below 4 keV (Boyarsky et al. 2007c). If one takes into account recent *lower* bound on the mass of sterile neutrino DM in the DW scenario $M_{\text{DM}} \geq 5.6$ keV (Viel et al. 2007), it seems that the possibility that all the DM is produced via DW scenario is ruled out (Boyarsky et al. 2007c). The possibility that only fraction of the DM is produced via DW mechanism remains open (Palazzo et al. 2007).

There exist other viable mechanisms of DM production, including e.g. resonant oscillation production in the presence of lepton asymmetries (Shi & Fuller 1999), or decay of the light inflaton (Shaposhnikov & Tkachev 2006). These mechanisms are currently not constrained and remain valid for DM particles with the masses in the keV range and above.

The search for the DM decay line signal produced by sterile neutrinos with masses above ~ 20 keV is complicated by the absence of the focusing optics telescopes (similar to *Chandra* or *XMM-Newton*) in the hard X-ray and γ -ray domain of the spectrum. For example, the existing restrictions in the 20 – 100 keV mass range (Boyarsky et al. 2006a,c) are derived from the observations of diffuse X-ray background, with the help of non-imaging instruments, HEAO-I (Gruber et al. 1999). The current status of astrophysical observations is summarized in Ruchayskiy (2007).

In this paper we use the spectrometer SPI on board of *INTEGRAL* satellite to put restrictions on parameters of decaying DM in the mass range 40 keV – 14 MeV. This range of masses is interesting, for example, the sterile neutrinos, produced in the early Universe in the presence of large lepton asymmetries (Shi & Fuller 1999) or through the inflaton decay (Shaposhnikov & Tkachev 2006). It is also relevant for the case of gravitino DM (Pagels & Primack 1982; Bond et al. 1982).

When the preparation of this paper was at its final stage, the work Yuksel et al. (2007) appeared, which used the results of Teegarden & Watanabe (2006) to put the restrictions on parameters of sterile neutrino DM in the range 40 – 700 keV. We will discuss it in more details in Section 6.

SPI spectrometer

The absence of the focusing optics significantly reduces the sensitivity of the telescopes operating in the hard X-ray/soft γ -ray energy band. Most of the instruments operating in this energy band use collimators and/or coded masks to distinguish signals from the sources on the sky from the instrumental background. Contrary to the focusing optics telescopes, both the source and background signals are collected from the entire detector, which significantly increases the irreducible background.

The focusing optics enables to significantly reduce the background only in the studies of point sources. If the source under investigation occupies a large fraction of the sky (e.g. the entire Milky Way galaxy), the performance of the focusing and non-focusing instruments with the same detector collection area are, in fact, comparable.

In the case of an extended source, emitting a narrow spec-

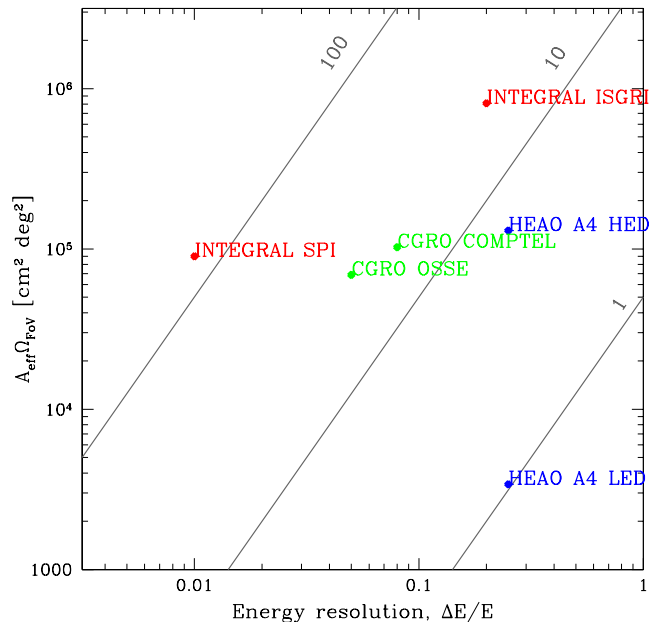


Figure 1. Comparison of sensitivity towards the search of the narrow DM decay line for different instruments with the wide FoV. Diagonal straight lines show the improvement of sensitivity (by a factor, marked on the line) as compared with the HEAO-I A4 low energy detector (LED), taken as a reference.

tral line, an efficient way of reduction of instrumental background is via the improvement of the spectral resolution of the instrument (in the case of a broad continuum background spectrum, the number of background counts at the energy of the line is proportional to the spectral resolution ΔE). The best possible sensitivity is achieved when the spectral resolution reaches the intrinsic width of the spectral line (see Fig.1 for the case of wide FoV instruments and Boyarsky et al. (2007b) for the case of narrow FoV instruments).

In the case of the line produced by the DM decaying in the Milky Way halo, the line width is determined by the Doppler broadening by the random motion of the DM particles. The velocity dispersion of the DM motion in the halo is about the rotation velocity of the Galactic disk, $v \sim 200$ km/s. This means that Doppler broadening of the DM decay line is about

$$\frac{\Delta E}{E} \sim \frac{v}{c} \simeq 10^{-3}. \quad (1)$$

Thus, the optimal spectral resolution of an instrument searching for the DM decay line produced by the Milky Way DM halo should be $\Delta E \simeq 10^{-3} E$.

Such optimal spectral resolution is almost achieved with the spectrometer SPI on board of *INTEGRAL* satellite, which has the maximal spectral resolving power of $E/\Delta E \simeq 500$ and works in the energy range 20 keV – 8 MeV (Vedrenne et al. 2003). SPI is a “coded mask” type instrument with an array of 19 hexagonal shaped Ge detectors (of which only 17 are operating at the moment).

The SPI telescope consists of a coded mask inscribed into a circle of the radius $R_{\text{mask}} = 39$ cm, placed at the height $H = 171$ cm above the detector plane and of the detector, which has the shape of a hexagon inscribed into a circle of the radius $R_{\text{det}} \simeq 15.3$ cm (see Fig. 2). The portion of the sky visible from each point of the SPI detector (the so-called *fully coded field of view*, FCFOV)

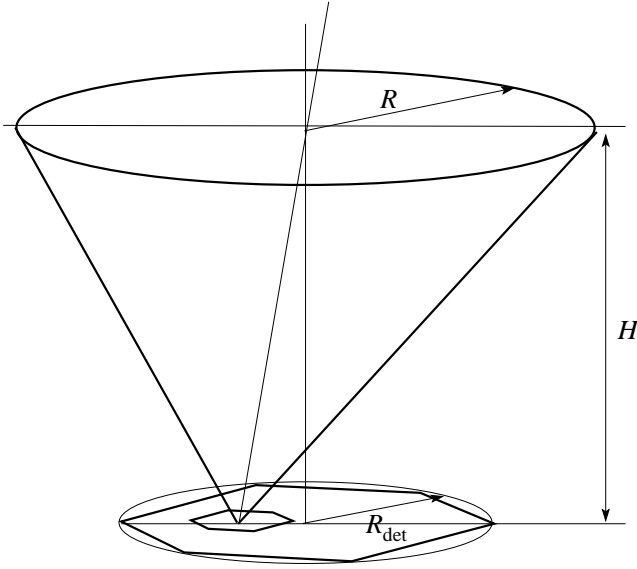


Figure 2. The geometry of the SPI FoV.

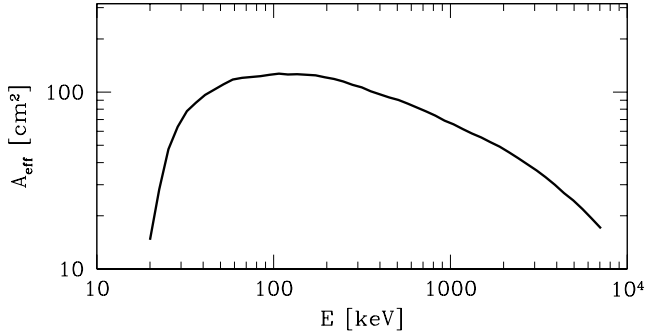


Figure 3. The effective area of the SPI detector for an on-axis source, as a function of the photon energy. The plot is produced by collective the on-axis effective areas of the 17 SPI detectors from the instrumental characteristics files.

has therefore angular diameter

$$\Theta_{\text{FCFOV}} = 2 \arctan \left[\frac{R_{\text{mask}} - R_{\text{det}}}{H} \right] \approx 16^\circ, \quad (2)$$

while the portion of the sky visible by at least some of the detectors (the *partially coded field of view*, PCFOV) is

$$\Theta_{\text{PCFOV}} = 2 \arctan \left[\frac{R_{\text{mask}} + R_{\text{det}}}{H} \right] \approx 35^\circ. \quad (3)$$

The solid angle spanned by the cone with this opening angle is $\Omega_{\text{PCFOV}} = 2\pi(1 - \cos(\Theta_{\text{PCFOV}}/2)) \simeq 0.29$ (see Fig. 2). Wide field of view makes the SPI telescope suitable for the study of the very extended sources, like the Milky Way DM halo.

2 THE EXPECTED SIGNAL FROM THE DM DECAY IN THE HALO OF THE MILKY WAY.

The expected surface brightness of the DM decay line in a given direction on the sky is a function of the angular distance ϕ between the given direction on the sky and the direction towards the Galactic

center (GC). It can be calculated by taking the integral of the DM density profile $\rho_{\text{DM}}(r)$ along the line of sight (“column density”)

$$S_{\text{DM}}(\phi) = \int_0^\infty dz \rho_{\text{DM}} \left(\sqrt{r_\odot^2 - 2zr_\odot \cos \phi + z^2} \right), \quad (4)$$

where $r_\odot \simeq 8.5$ kpc is the distance from the Solar system to the GC. Angle ϕ is related to the galactic coordinates (b, l) via

$$\cos \phi = \cos b \cos l. \quad (5)$$

Thus, the galactic center corresponds to $\phi = 0^\circ$, the anti-center $\phi = 180^\circ$, and the direction perpendicular to the galactic plane to $\phi = 90^\circ$. The expected DM flux is given then by

$$\frac{dF_{\text{DM}}(\phi)}{d\Omega} = \frac{\Gamma_{\text{DM}} E_\gamma}{4\pi M_{\text{DM}}} S_{\text{DM}}(\phi), \quad (6)$$

where Γ_{DM} is the DM decay rate

In general, the surface brightness $F_{\text{DM}}(\phi)$ is variable across the telescope FoV. This is especially true for a wide field of view (FoV) instruments (like SPI). In order to calculate the detector count rate, one has to integrate flux (6) over the FoV and over the (effective) detector area and then divide by the energy of the photons, $E_\gamma = M_{\text{DM}}/2$:

$$R = \iint_{\text{FoV}} d\alpha d\beta \frac{A_{\text{eff}}(E_\gamma|\alpha, \beta)}{E_\gamma} \frac{dF_{\text{DM}}(\phi(\alpha, \beta))}{d\Omega}, \quad (7)$$

where (α, β) are the angular coordinates in the FoV, A_{eff} is the effective area at energy E_γ for the photons, coming from the direction (α, β) .

The effective area of the SPI detector (which is determined by the transparency of the mask and the quantum efficiency of the detector) changes with the photon energy. For an on-axis point source,

$$dF/d\Omega(\alpha, \beta) = f_0 \delta(\alpha) \delta(\beta),$$

the integral of Eq. (7) reduces to $f_0 A_{\text{eff, on}}$, where $A_{\text{eff, on}}(E_\gamma)$ is the detector effective area for an on-axis source. Its dependence on energy E_γ is shown on Fig. 3.⁴

In the general case of extended sources, evaluation of the detector count rate (7) analytically is not possible because of the complicated dependence of the effective area on the off-axis angle (shown on Fig. 4). In the simplest case of an extended source with a constant surface brightness $dF_{\text{DM}}(\phi)/d\Omega = f_{\text{ext}} = \text{const}$, the integral of Eq. (7) reduces to the multiplication by the solid angle $\Omega_{\text{PCFOV}} \simeq 0.29$ and the effective area, averaged over the FoV:

$$\begin{aligned} A_{\text{eff, ext}}(E_\gamma) &= \frac{1}{\Omega_{\text{PCFOV}}} \iint_{\text{FoV}} d\alpha d\beta A_{\text{eff}}(E_\gamma|\alpha, \beta) \\ &\approx \kappa(E_\gamma) A_{\text{eff, on}}(E_\gamma). \end{aligned} \quad (8)$$

The numerical factor $\kappa(E_\gamma)$ depends on the energy and has to be calculated via a numerical integration over the energy dependent off-axis response map of the SPI detector. A reasonably accurate numerical approximation to $\kappa(E_\gamma)$ is given by

$$\kappa(E) \approx 0.165(E/\text{keV})^{0.11}. \quad (9)$$

One can see that $\kappa \ll 1$ in all the energy interval. This is explained by the fact that the detector area visible from a given direction on

⁴ The on-axis effective area is calculated by summing the energy-dependent on-axis effective areas of each of the 17 operating detectors of SPI, extracted from the instrument’s characteristics files.

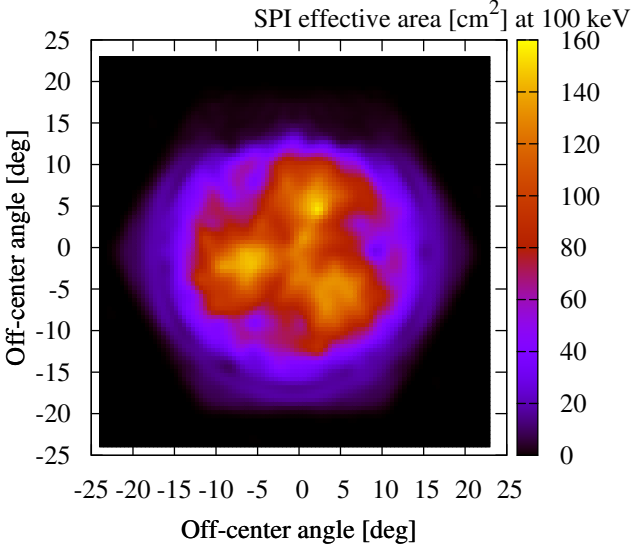


Figure 4. Dependence of the effective area on the off-axis position of a (point) source.

the sky strongly decreases with the increase of the off-axis angle of this direction, so that the sky-averaged effective area is much smaller than the on-axis effective area of the detector. Substituting (9), (8) into (7) one finds that for an extended source of constant surface brightness the detector countrate is

$$R_{\text{ext}} = 2.73 \times 10^{-5} \frac{\text{cts}}{\text{s}} \left[\frac{1 \text{ keV}}{E_\gamma} \right] \quad (10)$$

$$\times \left[\frac{A_{\text{eff,ext}}(E_\gamma)}{150 \text{ cm}^2} \right] \left[\frac{(dF_{\text{DM}}/d\Omega)_{\text{ext}}}{10^{-15} \text{ erg}/(\text{cm}^2 \text{ s sr})} \right] \quad (11)$$

2.1 Modeling the DM halo of the Galaxy

The DM halo of the Galaxy has been extensively studied (see e.g. Kravtsov et al. 1998; Klypin et al. 2002; Battaglia et al. 2005). Various DM profiles, used to fit observed velocity distributions, differ the most in the GC region.

It was shown in Klypin et al. (2002); Battaglia et al. (2005) that the DM halo of the MW can be described by the Navarro-Frenk-White (NFW) profile (Navarro et al. 1997)

$$\rho_{\text{NFW}}(r) = \frac{\rho_s r_s^3}{r(r+r_s)^2}, \quad (12)$$

with parameters, given in Table 1. The relation between virial parameters and ρ_s , r_s can easily be found (see e.g. the Appendix A of Boyarsky et al. 2007a).

To explore the uncertainty of the DM density profile in the inner part of the Galaxy, we also describe the DM distribution in the MW via an isothermal profile (Bahcall & Soneira 1980):

$$\rho_{\text{iso}}(r) = \frac{v_h^2}{4\pi G_N} \frac{1}{r^2 + r_c^2} = \frac{\rho_0}{1 + (r/r_c)^2}. \quad (13)$$

The following parameters of isothermal profile reproduce the DM contribution to the (outer parts of) Galaxy rotation curve $v_h = 170 \text{ km/sec}$ and $r_c = 4 \text{ kpc}$ (Boyarsky et al. 2006c, 2007a) (i.e.

$\rho_0 = 1.2 \times 10^6 \frac{\text{keV}}{\text{cm}^3} \left[\frac{v_h}{170 \text{ km/s}} \right]^2 \left[\frac{4 \text{ kpc}}{r_c} \right]^2$). These parameters are consistent with those, from favored NFW models of Klypin et al. (2002); Battaglia et al. (2005), i.e. for $\phi \geq 90^\circ$ the difference between isothermal model and NFW with preferred parameters was completely negligible (less than 5%) – c.f. FIG.5. Both types of models provide the local DM density at the position of the Sun to be $\rho_{\text{DM}}(r_\odot) \simeq 0.22 \text{ GeV/cm}^3$, which is close to the existing estimates (Kuijken & Gilmore 1989c,a,b, 1991; Gilmore et al. 1989).

The DM flux from a given direction ϕ , measured by an observer on Earth (distance $r_\odot \simeq 8.5 \text{ kpc}$ from the GC), is given by

$$S_{\text{iso}}(\phi) = \frac{\rho_0 r_c^2}{R} \times \begin{cases} \frac{\pi}{2} + \arctan\left(\frac{r_\odot \cos \phi}{R}\right), & \cos \phi \geq 0 \\ \arctan\left(\frac{R}{r_\odot |\cos \phi|}\right), & \cos \phi < 0 \end{cases}, \quad (14)$$

where $R = \sqrt{r_c^2 + r_\odot^2 \sin^2 \phi}$ and $\rho_0 r_c \simeq 1.5 \times 10^{28} \text{ keV/cm}^2$.

The uncertainty of the DM radial density profile in the inner Galaxy stems from the difficulty of separation between visible and DM contributions to the inner Galaxy rotation curve.⁵ In order to get the most conservative limit on the column density of the DM in the direction of the GC, one can assume the following “rigid lower bound”: while the DM *outside* the r_\odot is described by the “maximal disk” model (model A_2 of Klypin et al. 2002), for $r \leq r_\odot$ DM density remains constant (so that the total DM mass within r_\odot is the same as in the model A_2 of Klypin et al. 2002). This gives

$$\rho_{\text{DM}}^{\text{min}} \simeq 3.9 \times 10^6 \frac{M_\odot}{\text{kpc}^3} = 0.146 \times 10^6 \frac{\text{keV}}{\text{cm}^3}. \quad (15)$$

The surface brightness profile on the “constant density” model is shown in black dashed line on the Fig.5. One can see that the difference between the maximal ($\phi = 0^\circ$) and the minimal ($\phi = 180^\circ$) column densities is ~ 3.4 (as compared to ~ 6 for isothermal model). For comparison we show on Fig. 5 expected DM flux (6) for various profiles. The minimal column density is of course the one in the direction of anti-center: $S(\phi = 180^\circ) \simeq 0.33 \times 10^{28} \text{ keV/cm}^2$. We see that even for the minimal profile $S(\phi < 30^\circ) \geq 10^{28} \text{ keV/cm}^2$.

2.2 DM decay line count rate

In the case of the Majorana sterile neutrinos of the mass M_{DM} the DM decay width is given by (Pal & Wolfenstein 1982; Barger et al. 1995):⁶

$$\Gamma_{\text{DM}} \simeq 1.3 \times 10^{-32} \left[\frac{\sin^2 2\theta}{10^{-10}} \right] \left[\frac{M_{\text{DM}}}{1 \text{ keV}} \right]^5 \text{ s}^{-1}. \quad (16)$$

Substituting (16) to (6) on finds

$$\frac{dF_{\text{DM}}}{d\Omega}(\phi) \simeq 8.3 \times 10^{-15} \text{ erg}/(\text{cm}^2 \text{ s sr}) \quad (17)$$

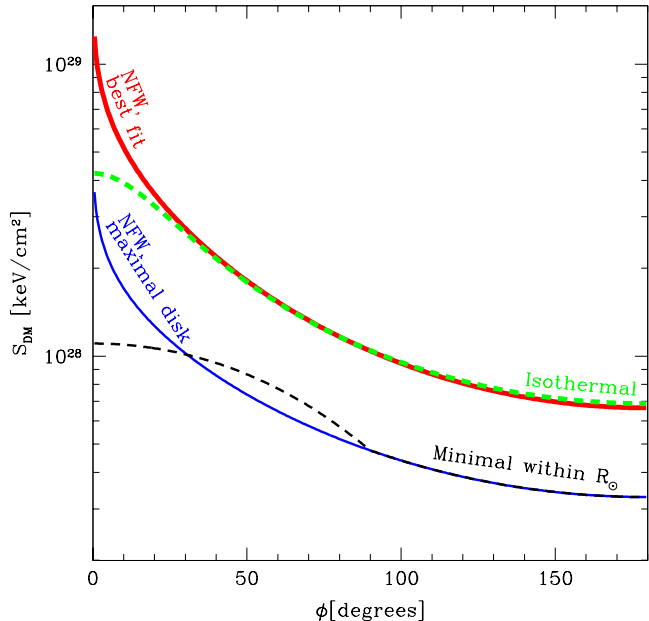
$$\times \left[\frac{\sin^2 2\theta}{10^{-10}} \right] \left[\frac{M_{\text{DM}}}{1 \text{ keV}} \right]^5 \left[\frac{S_{\text{DM}}(\phi)}{10^{28} \text{ keV/cm}^2} \right]$$

⁵ When quoting results of Klypin et al. (2002), we do not take the effects of baryon compression on DM into account. While these effects make DM distribution in the core of the MW denser, any such computation is strongly model dependent.

⁶ The quoted value of Γ_{DM} is for the Majorana sterile neutrino. In case of Dirac particle this value is 2 times smaller (c.f. Pal & Wolfenstein 1982; Barger et al. 1995).

Table 1. Best-fit parameters of NFW model of the MW DM halo. Max. disk model maximizes amount of baryonic matter in the inner 3 kpc of the MW halo ($M_{\text{DM}}/(M_{\text{disk}} + M_{\text{bulge}}) = 0.4$ for the model A_2 and $M_{\text{DM}}/(M_{\text{disk}} + M_{\text{bulge}}) = 0.14$ in the model B_2).

References	$M_{\text{vir}} [M_{\odot}]$	$r_{\text{vir}} [\text{kpc}]$	Concentration	$r_s [\text{kpc}]$	$\rho_s [M_{\odot}/\text{kpc}^3]$
Klypin et al. (2002), favored models (A_1 or B_1)	1.0×10^{12}	258	12	21.5	4.9×10^6
Klypin et al. (2002), Max. disk models A_2	0.71×10^{12}	230	5	46	0.6×10^6
Klypin et al. (2002), Max. disk models B_2	0.71×10^{12}	230	10	23	3.1×10^6
Battaglia et al. (2005)	$0.8_{-0.2}^{+1.2} \times 10^{12}$	255	18	14.2	11.2×10^6

**Figure 5.** Expected column density for various DM profiles: favored NFW profile (red thick solid line); NFW profile with the maximal disk (model A_2 , see Table 1) – blue solid line; cored (isothermal) profile – green thick dashed line; constant density within r_{\odot} – black dashed line.

The lower bound on the DM decay line rate in SPI pointings toward the inner Galaxy is calculated by substituting the column density $S = 10^{28}$ keV/cm² (see Fig. 5) into Eqs. (10), (17)

$$F_{\text{min}} \simeq 3.0 \times 10^{-6} \frac{\text{cts}}{\text{cm}^2 \text{ s}} \left[\frac{S_{\text{DM}}(\phi)}{10^{28} \text{ keV/cm}^2} \right] \left[\frac{\sin^2 2\theta}{10^{-10}} \right] \left[\frac{M_{\text{DM}}}{1 \text{ keV}} \right]^4 \quad (18)$$

The approximation of the constant surface brightness works well, if the extended source has a core of the angular diameter exceeding the size of the SPI partially coded FoV ($\Theta_{\text{PCFOV}} \approx 17^\circ$ maximal off-axis angle). Taking isothermal profile the angular size of the flat core of the extended source is

$$\phi_{\text{core}} = \arctan(r_c/r_{\odot}) \simeq 25^\circ, \quad (19)$$

which satisfies this constraint.

3 STRATEGY OF SEARCH FOR THE DM DECAY LINE WITH SPI

The MW halo contribution to the DM decay signal represents the all-sky source. Indeed, as the results of Section 2.1 show, the variability of the signal over the sky may be as low as the factor ~ 3 . This makes the strategy of search of the DM decay signal different from any other types of astrophysical sources: the point sources, diffuse sources (e.g. $\sim 10^\circ$ Gaussian profile for e^+e^- annihilation

region, Knödseder et al. (2005)) or even the search for DM annihilation signal (see e.g. Tasitsiomi et al. 2004; Boehm et al. 2004; Diemand et al. 2007; Sánchez-Conde et al. 2006; Carr et al. 2006).

The problem gets exacerbated by the fact that during its motion, SPI is irradiated by the charged high-energy particles (particles from Earth radiation belt, Solar wind, cosmic TeV photons). As a result, the materials (even detectors themselves) used for SPI construction start to radiate in different energy regions (see subsection 3.2). As a result any SPI spectrum consists of a broad continuum, which is a combination of the sky and instrumental backgrounds, and of a set of the instrumental background lines (Attié et al. 2003; Diehl et al. 2003; Jean et al. 2003; Weidenspointner et al. 2003). In order to detect a spectral line produced by an astrophysical source one has to be able to (a) separate the continuum and line contributions to the spectrum and (b) separate the instrumental and sky signal contributions to the lines found.

One can expect three *a priori* situations:

- (I) DM decay line is strong (its *equivalent width* much larger than the spectral resolution) and at its position there are no other strong lines (of either instrumental or astrophysical origin). Such a line, due to its presence in any SPI spectrum and its low variability over the sky can in principle be confused with some unknown instrumental line.
- (II) DM line is weak ($\sim 3 - 4\sigma$ detection over the continuum) but its position also does not coincide with any instrumental line.
- (III) DM decay line coincides with some instrumental line. To be able find such a line we need to model SPI instrumental background.

To be able to work effectively with all these situations, we need to find the way to separate the source and background contributions.

3.1 Imaging

To distinguish source and background contribution to the signal, one often uses imaging capabilities of an instrument. If the size of a point or even an extended source on the sky is smaller than the size of the SPI FoV one can (at least, to some extent) use the imaging capabilities of the SPI instrument. In this case the coded mask, placed above the detector, partially screens the individual detectors from the source, so that the source at a given position on the sky produces different countrates in different detectors. One can find the source flux by comparing the ratios of the actual countrates in different modules of the detector to the ones predicted by the degree of screening of the modules by the mask (see Dubath et al. 2005; Skinner & Connell 2003). It is a challenge, however, to use the imaging capabilities of the SPI to separate the astrophysical signal from the instrumental background if the size of the extended source is comparable to the size of the SPI FoV (see e.g. Knödseder et al. 2005; Allain & Roques 2006; Weidenspointner et al. 2007, and refs. therein). Therefore for our

analysis we did not use any imaging capabilities of SPI, and to produce spectra from some point in the sky we just collected all the photons, arriving in the SPI FoV.

3.2 SPI background modeling

In the absence of imaging, the separation of the instrumental and astrophysical contributions to the line spectrum requires some sort of background modeling (see e.g. Weidenspointner et al. 2003; Teegarden et al. 2004; Teegarden & Watanabe 2006). Namely, for the background modeling we can use the fact that for any DM distribution model the intensity of the DM decay line changes by a factor ≥ 3 between the pointings towards the Galactic center ($\phi \sim 0^\circ$) and anti-center ($\phi \sim 180^\circ$, see Sec.2.1). On the other hand, if the line is of purely instrumental origin, there is no *a-priori* reason why the strength of the line in the background spectra of the pointings towards e.g. the Galactic Anti-center should be different from the strength of the line in the spectra of the pointings toward e.g. the GC. Thus, one possible way to distinguish between the DM decay and instrumental origin of the line is to study the variations of the line’s strength depending on its sky position (in the simplest case – on the “off-GC” angle ϕ , of the pointing, Eq. (5)).

The situation becomes more complicated due to the fact that the instrumental background (and thus the intensity of the instrumental lines) experiences great variability in time (depending on the position in orbit, solar flares and the solar activity period, degradation of the detectors, etc., c.f. Jean et al. 2003; Teegarden et al. 2004). As observations of different parts of the sky can be significantly separated in time, one needs to use “background tracers” to find the correct spatial dependence of the line intensity (Jean et al. 2003; Teegarden & Watanabe 2006). Without some sort of “renormalization” procedure, which corrects the absolute value of the line flux using a measurement of a specific characteristics of the SPI instrument as a “calibrator” of the flux, the ϕ dependence for any of the detected lines contains no useful information. There exist various “background tracers” (Ge detectors saturation rates, anti-coincidence shield rates, rates of certain background lines, see Jean et al. (2003); Teegarden et al. (2004); Teegarden & Watanabe (2006) and refs. therein).

3.3 Searching for the lines

To be able to detect strong DM line, which is not close in position to any instrumental line (case **I** above), we used the modification of the method of background subtraction, described in Teegarden & Watanabe (2006, hereafter **TW06**). TW06 looked for the γ -ray lines, assuming different types of sources, from the point ones to the very diffuse (10° Gaussian, 30° flat, etc.) TW06 showed that the strong background line at 198 keV can be used as a background tracer, if one matches background observations to be close in time to the corresponding “source” ones. This allowed TW06 to cancel all strong instrumental lines with the precision better than 1%. TW06 detected *no* emission line in such background subtracted spectrum (apart from the 511 keV and 1809 keV) with the significance above 3.5σ .

We adopt the following modification of the TW06 method:

- As the DM decay signal remains nearly constant within central $30 - 50^\circ$, the method of TW06, if applied directly, could cancel

most of the DM signal.⁷ We therefore subtract the data (renormalized by the strength of 198 keV line) in the direction *away* from the GC (off-GC angle $\phi > 120^\circ$) from the ON-GC dataset (the angle $\phi \leq 13^\circ$).

- In the resulting “ON–OFF” spectrum we perform the search for the line with the significance higher than 3σ .

This procedure allows to eliminate strong instrumental lines with the precision better than few percents. At the same time any strong DM line would remain in the “ON–OFF” spectrum. Indeed, even for the flattest profile (Section 2.1), the strength of the DM signal in the OFF dataset is *at least* 60% weaker that of the ON dataset. Therefore we see, that the modification, described above, is indeed well suited for searching of the strong DM decay line (case **I**).

However, this method does not work well for the weak ($3-4\sigma$) lines, or for the lines, whose position coincides with some instrumental line (cases **II-III** above). Indeed, in this case it is not possible to tell whether the remaining line is the residual of the instrumental one or has the astrophysical origin. Below we will use an alternative method of analysis of the detected lines, suitable for cases **II** and **III**.

3.4 Analyzing a candidate line

Having detected a number of lines with the significance of 3σ and above, we should decide which of them can be considered as “DM decay line candidates”. To this end we do the following.

- a) We compare line flux for each of these lines with the flux of the same line in the “ON” spectrum. We decide that the line is a “DM line candidate” if the cancellation of the flux between ON and OFF datasets was worse than 10%.⁸

- b) For any “DM candidate line” we construct its “spatial profile” (as described in details in the next Section) to check for the possibility of it to be a DM decay line (we also construct distribution of the line flux over the sky for all the unidentified lines from Weidenspointner et al. 2003). Since the column density of the DM in the direction toward the GC should be higher than that of in the direction toward the Galactic anti-center, one should see a gradual decrease of the line strength with the increasing angle ϕ . We do not make any specific assumption about the DM density profile and do not try to fit the candidate line spatial profile to any particular model, but rather look if there is a general trend of decreasing intensity of the line with the increasing off-GC angle.

4 DATA REDUCTION

4.1 ON dataset

During its almost 5 years in orbit *INTEGRAL* has intensively observed the inner part of the Galaxy (Galactic Center, Galactic Bulge and the inner part of the Galactic Plane) and collected about $T_{\text{exp}} \sim 10$ Ms of exposure time in the GC region. In our analysis of the inner Galaxy we used the publicly available data (as of July

⁷ For example for the most conservative DM distribution model, the difference of DM signals at $\phi = 0^\circ$ and $\phi = 30^\circ$ is mere 8%.

⁸ In principle, the DM line in ON–OFF spectrum should not cancel by more than $\sim 40\%$, while the background instrumental line should cancel better than 1%. Thus the choice of the threshold to be around 10% ensures that no DM decay line was thrown away while most of the instrumental lines disappeared.

2007) from all *INTEGRAL* pointings at which the angle off the GC was at most 13° and for which the SPI exposure time was larger than 1 kses. This criteria selects 5355 pointings (or ‘‘Science Windows’’, ScW), with total exposure time of 12.2 Ms, spread over the period from February 2003, till April, 25, 2006. We call this dataset ‘‘ON’’ dataset.

For each of the analyzed ScWs, we have extracted photon (event) lists from `spi-oper.fits` files and applied additional energy correction to convert the channel number into photon energy, using `spi_gain_cor` tool from standard Offline Analysis Software (OSA). We have binned the events into narrow energy bins of the size $\Delta E_{\text{bin}} = 0.5$ keV to generate the background counts spectra in each ScW, each revolution and, subsequently, in the entire data set.

We then applied the ‘‘sliding spectral window’’ method to the line search (as described e.g. in TW06 to produce a continuum subtracted spectrum of the ‘‘ON’’ dataset. Namely, at each given energy E_0 , one defines an energy interval $E_0 - 2\Delta E < E < E_0 + 2\Delta E$, where ΔE is the SPI spectral resolution at a given energy, as a ‘‘line signal’’ energy band. For the (energy dependent) ΔE we used approximate formula from SPI/*INTEGRAL* ground calibration of FWHM (Attie et al. 2003):

$$\Delta E(E) = F_1 + F_2\sqrt{E} + F_3E \quad (20)$$

where $F_1 = 1.54$, $F_2 = 4.6 \cdot 10^{-3}$, $F_3 = 6.0 \cdot 10^{-4}$ and energy E is in keV. For $E = 10^3$ keV $\text{FWHM} \approx 2.3$ keV.

For each energy bin centered at an energy E_0 we have defined the two adjacent energy intervals, $E_0 - 4\Delta E < E < E_0 - 2\Delta E$ and $E_0 + 2\Delta E < E < E_0 + 4\Delta E$, and postulated that the sum of the countrates in these two adjacent energy bands gives the measure of the continuum count rate in the energy band around E_0 . Subtracting the sum of the countrates in the adjacent energy bands from the countrate in the ‘‘line signal’’ energy band, we have calculated the continuum subtracted countrate at a given energy E_0 . Doing such procedure at all the energies $20 \text{ keV} < E_0 < 8 \text{ MeV}$, we have produced a ‘‘continuum subtracted’’ SPI background spectrum. In this spectrum we were able to identify most of the known instrumental lines (Weidenspointner et al. 2003).

4.2 ON–OFF dataset

Most of the lines found in the continuum subtracted background spectrum are of the instrumental origin. To remove them, we matched each ScW in the ON dataset with the pointing *away* from the GC (galactic coordinate $\phi > 120^\circ$) – OFF pointing. As described by TW06, the 198 keV line can serve as good background tracer if the time duration between ON and OFF observations is ≤ 20 days. We were able to match 3688 ON–OFF pairs. For each ON–OFF pair we introduced normalizing coefficient n for the OFF spectrum in such a way that the strong instrumental line at 198 keV cancels completely after subtraction of the OFF spectrum multiplied by the factor n from the ON spectrum. After that we subtracted (renormalized) OFF ScW from the corresponding ScW from the ON dataset. This allowed us to remove most prominent instrumental lines with the precision better than 1% (c.f. Fig. 6). To avoid contributions of strong astrophysical sources (such as e.g. Crab) we threw out all pairs with negative total flux at 20–40 keV range after subtraction. Taking average over 2456 remaining ‘‘good’’ pairs we received the spectrum almost free from background at energies above 200 keV. At low (< 200 keV) energies we found continuum component, which can be fitted with the simple

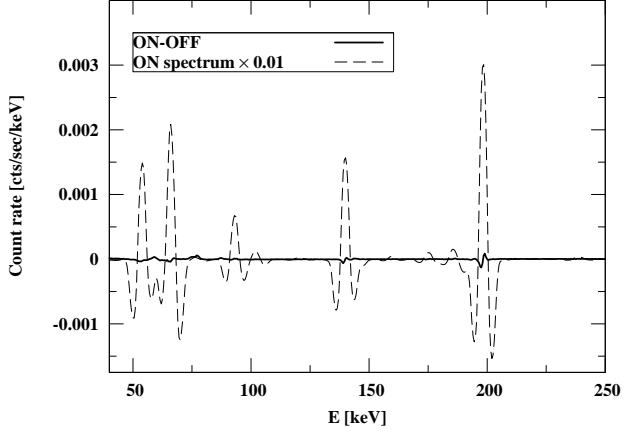


Figure 6. Comparison of ON–OFF spectrum (thick solid line) with the $0.01 \times$ the ON spectrum after the sliding window (thin dashed line). It can be seen that the instrumental lines are subtracted with the precision better than 1%.

powerlaw:

$$F(E) = F_0 \left[\frac{E}{100 \text{ keV}} \right]^\alpha \quad (21)$$

Parameters of this background were found to be

$$\begin{aligned} F_0 &= (4.95 \pm 0.05) \times 10^{-5} \text{ cts/s/cm}^2 \\ \alpha &= -(2.264 \pm 0.003) \end{aligned} \quad (22)$$

This continuum represents the residual contribution from all the set of the astrophysical sources present in the Galactic Bulge.

4.3 Systematic error

To estimate the systematic error of our ‘‘ON-minus-OFF’’ dataset, we computed background around the ‘‘tracer line’’ of 198 keV. We found that it does not vanish. Thus, we estimated the systematic error as the error in the normalization coefficient n which would make the background zero within systematic uncertainty. This correction δn can be found as follows. Let n be the coefficient, needed to cancel flux in the 198 keV line in ON and OFF spectra:

$$n = F_{ON}/F_{OFF} \quad (23)$$

where F_{ON}, F_{OFF} – fluxes in 198keV line in ON and OFF ScWs correspondingly. The remaining non-zero δF flux in the adjacent to line position in ON–OFF spectrum, determines the uncertainty of the coefficient:

$$\delta n = \frac{\delta F}{F_{ON}} \quad (24)$$

We found, that average value of $\langle \delta n \rangle$ is equal to $\langle \delta n \rangle = 1.1 \cdot 10^{-3}$, $\langle n \rangle \sim 1$. So, our systematic error of final ON–OFF spectra at energy E is $1.1 \cdot 10^{-3} F_{OFF}(E) \approx 1.1 \cdot 10^{-3} F_{ON}$. We add this systematic uncertainty to the flux of ON–OFF spectrum in every energy bin.

4.4 Obtaining 3σ restrictions

At the energies at which no lines were detected (i.e. the ‘‘continuum subtracted’’ count rate did not deviate by more than 3σ from zero) we obtained the 3σ upper limit on the possible flux from the DM

Phase	Revolutions (start-stop)
1	042–092
	096–140*
2	140–205
	209–215*
3	215–277
4	282–326
5	330–395
6	400–446

Table 2. Splitting revolutions into phases in correspondence with annealing phases and breakage of the detectors (revolutions, marked with the *).

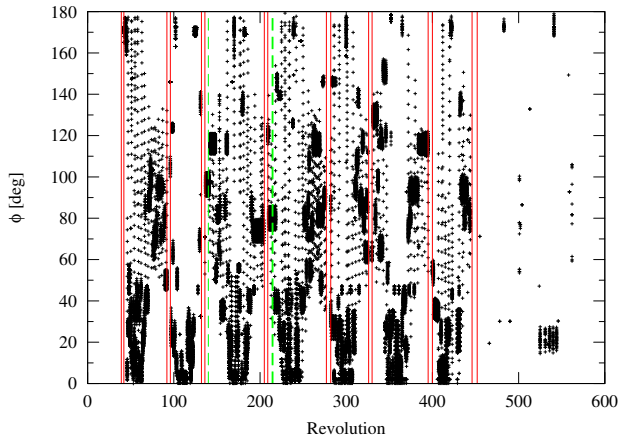


Figure 7. Position on the sky as a function of revolution over 6 years of *INTEGRAL* observations. The periods of annealing phases are shown in solid vertical lines. Two dashed lines indicate the revolution, during which 2nd and 17th of 19 SPI detectors have failed.

decay. Above ~ 200 keV the flux in the energy bin is zero within statistical errors, therefore 3σ upper limit flux is given by statistical plus systematic errors. Below 200keV we put statistical restrictions above powerlaw continuum flux (21), described in the Section 4.2. Using Eq. (18) one can derive the restriction on the sterile neutrino mixing angle, implied by this upper limit. One should also take into account that the subtraction of the OFF observations led to the reduction of the expected DM signal. Taking the most conservative “minimal” model, described in Section 2.1, we see that the subtraction of the OFF signal leads to about 40% decrease of the expected DM signal.⁹ The resulting 3σ bound is shown on Fig.10.

4.5 Possible DM candidates

When analyzing ON–OFF spectrum, we found that almost all lines, present in ON spectrum cancel with precision better than few percents. We found 21 lines that did not cancel by at least 90%, (including known lines at 511 keV and 1809 keV). Apart from these 2 lines all other lines are detected with low significance $3-4\sigma$.

As discussed in Sections 3.3–3.4, we took all these lines as possible DM candidates and analyzed the dependence of the line fluxes $F(\phi)$ on the off-GC angle ϕ of the pointing. If the DM distribution in the inner part of the Galaxy were known, it would be possible to distinguish between the instrumental and DM decay origin of a line by fitting $F(\phi)$ with a known profile calculated from

⁹ To estimate this, we took the maximal column density for OFF observations at $\phi = 120^\circ - 17^\circ$.

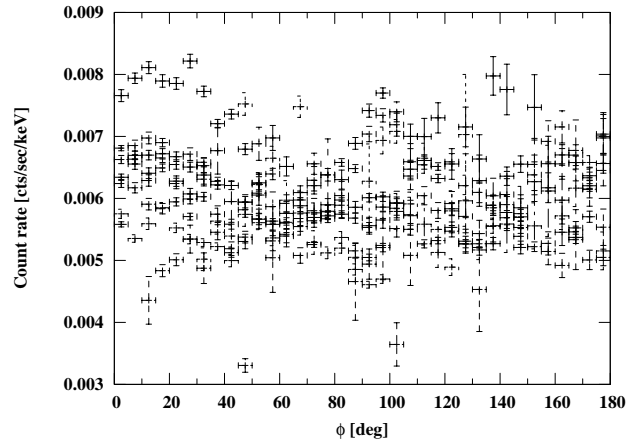


Figure 8. Scatter of the flux data points for the line at $E = 1068$ keV as a function of the off-GC angle.

the radial DM density profile. However, the details of the radial DM density profile in the inner Galaxy are highly uncertain, and this prevents us from directly fitting the model profile to the data. We adopted a simple criterion which selects a DM decay candidate line: the ratio of fluxes

$$\mathcal{R} = \frac{F(0^\circ)}{F(180^\circ)} \geq \mathcal{R}_{min} \simeq 3. \quad (25)$$

where \mathcal{R}_{min} is the ratio of the DM decay line fluxes from the GC and the Galactic anti-center in the “minimal DM content” model of DM distribution.

Since the observations at different off-GC angles are done during different time periods, to properly study the dependence of the line flux on the off-GC angle ϕ one should take into account the time variability of the response of the SPI detectors. Several factors have to be taken into account. First, the SPI instrument goes through a so-called “annealing” phase – heating of the detectors to recover from a radiative damage.¹⁰ Next, two of the 19 SPI detector have “died”.¹¹ The failed detectors also affect the response of their neighbors. To magrinalize the effects of the changing response of the SPI detector, we split the entire data set into 7 periods, as shown on Fig. 7. The intervals are summarized in the Table 2. As both detector failures occurred soon after the end of an annealing phase, we chose to ignore revolutions 136 through 140 and 209 through 215. The period 096–140 does not cover the essential part of the sky and therefore we skip it, leaving only 6 periods.

For each of the periods, shown in the Table 2, we plot the distribution of the line flux as a function of the off-GC angle ϕ . The results are summarized on Fig. 13, p. 15. One can see that none of these lines exhibits clear trend of decreasing from $\phi = 0^\circ$ towards $\phi = 180^\circ$. For each line (and each phase) we also compute the average flux \bar{F} , standard deviation σ_F from the average, minimum (F_{min}) and maximum (F_{max}). Our analysis shows that (a) 95–100% of all points lie within $3\sigma_F$ from the average (thus, the data is consistent with having flat spatial profile) and (b) the scatter of the data ($F_{max} - F_{min}$) is much less than its mean value $\langle F \rangle$. Therefore, none of them cannot originate entirely from a DM decay. The corresponding numbers for each line and each phase are summarized in Table 4, page 16.

¹⁰ For details see SPI User Manual:

http://isdc.unige.ch/Instrument/spi/doc/spi_um.

¹¹ Detector # 2 at revolution 140 and detector #17 at revolutions 214–215.

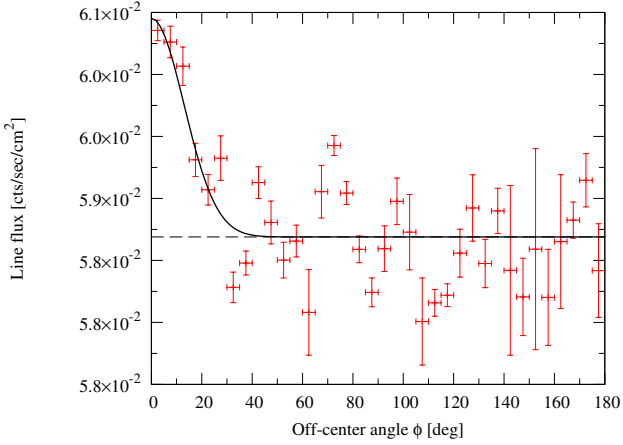


Figure 9. Dependence of the intensity of the positron annihilation line at $E = 511$ keV on the off-GC angle. The solid line shows fit to the data in the form $\text{const} + Ne^{-\phi^2/(2\sigma^2)}$.

The positron annihilation line at $E = 511$ keV illustrates a situation, when a line of astrophysical origin is superimposed on top of the strong instrumental line. In this case, the data can be fitted by the constant, plus some function, depending on assumed shape of the source. Fig. 9 shows the dependence of the flux of the 511 keV line on the off-GC angle of the SPI pointing. One can see that for the pointings with the off-GC angle less than 20° (about the size of the PCFOV of SPI) the 511 keV line flux contains a contribution from a sky source at the position of the GC, while for the pointing at larger off-GC angles the astrophysical source is not visible and the only contribution comes from the instrumental line, whose flux does not depend on the off-GC angle of the pointing.

5 RESULTS

We analyzed the spectrum of SPI and found that none of the strong (i.e. detected with significance above 5σ) lines can be interpreted as that of the decaying DM. This conclusion was based on the fact that variability of these lines over the sky is less than 10% (when moving from GC to the anti-center). At the same time for any realistic DM model such a variability would be greater than at least 60%. Thus, we exclude the possibility that one of the spectral lines, detected in the SPI background spectrum is a DM decay line.

The non-detection of a DM decay line in the entire energy range of the SPI detector has enabled us to put an upper limit on the parameters of the DM particles. In particular, the 3σ upper bound on the mixing angle of the sterile neutrino DM in the mass range 40 keV – 7 MeV is shown on Fig. 10, p. 12.

Our results are applicable to any decaying DM (e.g. gravitino). To this end we also present the restrictions on the DM life-time (with respect to the radiative decay) as a function of the energy of emitted photon. The corresponding exclusion plot is shown on Fig. 11.

To present our results in the form less dependent on a particular model of DM distribution in the MW, we show the 3σ sensitivity towards the line search on Fig. 12. Note, that these results should be used with care, as the sensitivity depends on the assumed spatial profile of the source (because the effective area decreases with the off-axis angle, see discussion in Section 2). The results, presented on Fig. 12 are valid for an extended source with the surface brightness which varies on the angular scales larger than (or comparable

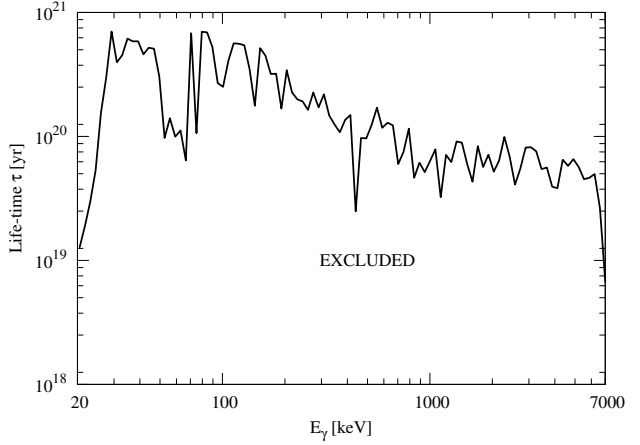


Figure 11. Life-time of the radiatively decaying DM as a function of the emitted photon energy. Region below the curve is excluded.

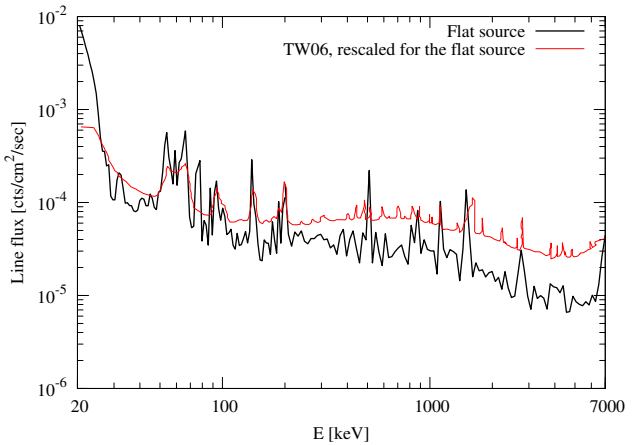


Figure 12. 3σ sensitivity towards the line search in case of the flat diffuse source (thick black line). The results of Teegarden & Watanabe (2006, Fig. 9), (rescaled to account for sensitivity towards the flat diffuse source, rather than 10° Gaussian) are shown in thin red line.

to) the size of the SPI field of view (black solid line). This plot is analogous to the Fig. 9 of Teegarden & Watanabe (2006) (TW06). However, a direct comparison of the Fig. 9 of TW06 and Fig. 12 is not possible, since TW06 have assumed a different morphology of the extended source (10° Gaussian). Explicitly taking into account the dependence of the effective area of the SPI detector on the off-axis angle (see Section 2), one can find that in order to make a direct comparison between the two figures, one has to “re-scale” the results of Fig. 9 of TW06 by an (energy dependent) factor of ≈ 1.5 . This factor converts the sensitivity for the line, produced by a source with the Gaussian surface brightness profile, into the one produced by a source of approximately constant surface brightness (see red curve in Fig. 12).

We have found a number of weak (with the significance $3-4\sigma$) lines in the background-subtracted spectrum of SPI. These lines cancel by worse than 90% when subtracting OFF dataset (see Section 4). Apart from it we have found in the background-subtracted spectrum two lines with high significance – known lines at 511 keV and at 1809 keV. Any of these lines can in principle be a DM decay line. We analyzed each of them, by considering the profile of their intensity over the sky. Our analysis shows that none

E [keV]	Sign., σ	ΔE [keV]	Identification
68.5	11.4	0.65	66.7 Ge complex
76.5	58.8	1.10	75 Bi K_α
87	21.2	0.90	87 Bi K_β
94	5.2	0.55	91-105 GaZn
134.5	15.5	0.90	132-140 Ge complex
143	12.6	1.20	140-147 Ge complex
177	3.9	0.95	175 AsGe
186.5	7.3	1.10	184.6 GaZn
193	24.8	0.75	190-198 Ge complex
200	29.3	0.60	198-215 Ge complex
205.5	5.4	0.50	198-215 Ge complex
240	3.4	1.10	238 PbBi
302	3.9	0.70	301.5 GaZn
311.5	7.4	1.10	309.8 GaZn+K
330.5	3.2	0.55	328=? or 331=PbTl
385.5	3.2	1.45	383=PbTl or ??
404.5	5.5	0.95	403 Ga Zn+K
431.5	4.4	0.55	??
440.5	12.4	0.80	438 ZnZn
465	4.3	0.95	470-485 NaNa
511 [†]	52.5	1.25	511 e^+e^-
576	5.2	0.95	574 GeGa
585.5	7.2	1.10	584.5 GeGa+K
597.5	5.0	1.45	596-610 Ge complex
754	4.7	0.85	751 BiBi
803.5	3.7	0.75	803 BiPb
812	10.6	0.95	810 CoFe
819.5	11.6	0.85	817 CoFe+K
827.5	7.1	0.75	825 PbPb
836	12.1	0.95	834 MnCr
845	6.5	1.30	843 MgAl
874	8.8	1.05	872 GeGa
884	10.0	1.05	882 GeGa+K
913	5.2	1.05	911 AcTh
937 [†]	3.1	0.95	?? or 935=MnCr

E [keV]	Sign., σ	ΔE [keV]	Identification
990	6.0	0.85	987 PbPb
947 [†]	3.6	1.50	??
1014.5	11.1	1.40	1014 MgAl
1068.5	3.3	1.40	?? or 1063=PbPb
1079	3.3	1.00	1077=GaZn
1098	6.8	1.05	1095=?
1108.5	19.9	1.05	1106 GeGa
1118.5	23.9	1.05	1117 GeGa+K
1127	23.5	0.85	1124.5 ZnCu+K
1234 [†]	4.5	1.40	1231 TaW
1349.5	3.5	0.80	1347 GeGa+K
1368.5	13.2	1.55	1368 NaMg
1719.5 [†]	3.3	1.55	1719 BiPb
1753.5	4.0	1.45	?? or 1758=?
1767.5	11.1	1.40	1764 BiPb
1781.5	12.4	1.45	1778 AlSi
1809 [†]	15.2	1.85	1808 Mg
1904	3.2	1.45	1901=GeGa+K or ??
2212	6.7	2.20	2195-2223 BiPo, Al
2225	5.4	1.10	2223 HD
2322	3.1	1.55	2319=?
2583.5	3.5	1.65	2599=? or ??
2616	5.0	1.90	2614 PbTl
2756	9.5	1.90	2754 NaMg
3002.5	5.1	2.45	2993-3013 Al
3176.5 [†]	3.4	1.95	??
3331 [†]	3.4	2.05	??
3802	3.6	2.10	3800 GaZn+K
4307.5	3.6	3.40	4304 GaZn+K
4454	4.2	8.45	4434 C
4738 [†]	3.5	2.30	??
5186.5 [†]	3.5	2.20	??
5208.5 [†]	4.0	1.95	??
5757 [†]	3.4	2.95	??
6129	20.5	3.25	6128.9 O

Table 3. Lines, detected in the ON-OFF spectrum with the significance $\geq 3\sigma$. Lines, marked with [†] cancel worse than by 90% in the ON-OFF spectrum (as compared with their flux in ON spectrum) and thus represent a “DM candidates”. The “Identification” column indicates the probable identification of the line in Weidenspointner et al. (2003). Lines, marked with “?” are not identified in Weidenspointner et al. (2003), lines marked with “??” are not present in Weidenspointner et al. (2003).

of these lines could be *pure* DM line (as their dependence on the off-GC angle does not show any clear trend to decrease towards the anti-center). The possibility that some of these lines are the superposition of instrumental and DM lines remains open. Quantitative analysis of the amount of DM flux admissible in a given line depends strongly on the model of the DM distribution in the Milky Way halo. Therefore it was not conducted here.

6 DISCUSSION

The purpose of this work was to understand how to search for the DM decay line with the SPI spectrometer and to check that none of the strong lines, present in the SPI background, was confused with the DM decay line. Our analysis shows that all the strong lines were, indeed, of instrumental origin and provides the upper bound on the flux of “weak” ($3-4\sigma$ above the background) lines, which leads to the corresponding restrictions (see Sec. 5). To further improve the results, one needs to work with the weak lines (or lines, coinciding in position with instrumental ones). To do this one needs more sophisticated procedures of subtraction of the instrumental background, such as e.g. imaging.

One of the most interesting cases of the coinciding instru-

mental and celestial line is the positronium annihilation line at 511 keV. An excess of positron annihilation emission on top of the strong instrumental line (related to positrons annihilating inside the detector) was noticed long ago (for an incomplete set of references see e.g. Prantzos 1993; Milne et al. 1999; Cheng et al. 1997; Purcell et al. 1997; Knödlseeder et al. 2005; Weidenspointner et al. 2006, 2007). There exist many attempts of explanation of this excess. In particular, it was attributed to the annihilating or decaying DM (see e.g. Boehm et al. 2004; Hooper et al. 2004; Boehm et al. 2006; Frère et al. 2007; Picciotto & Pospelov 2005; Rasera et al. 2006). The sterile neutrino DM with the mass $m_s > 1$ MeV possesses decay channel $N_s \rightarrow e^+e^-\nu$, with positrons annihilating either in flight or at rest, by forming the positronium atom (see e.g. Beacom & Yüksel 2006; Sizun et al. 2006). Thus, it is possible that the decay of sterile neutrino DM contributes to such a line. The detailed analysis of this case will be reported separately.

It should be also mentioned, that the region of masses between $20 \text{ keV} \lesssim m_{\text{DM}} \lesssim 40 \text{ keV}$ remains inaccessible for the existing X-ray missions. The strongest restrictions in this region were produced, using the data of HEAO-1 mission (Boyarsky et al. 2006c).

When the work on this paper was at its final stage, the work Yüksel et al. (2007) (Y07 in what follows) appeared. Y07 obtained the restrictions on parameters of sterile neutrino in the range

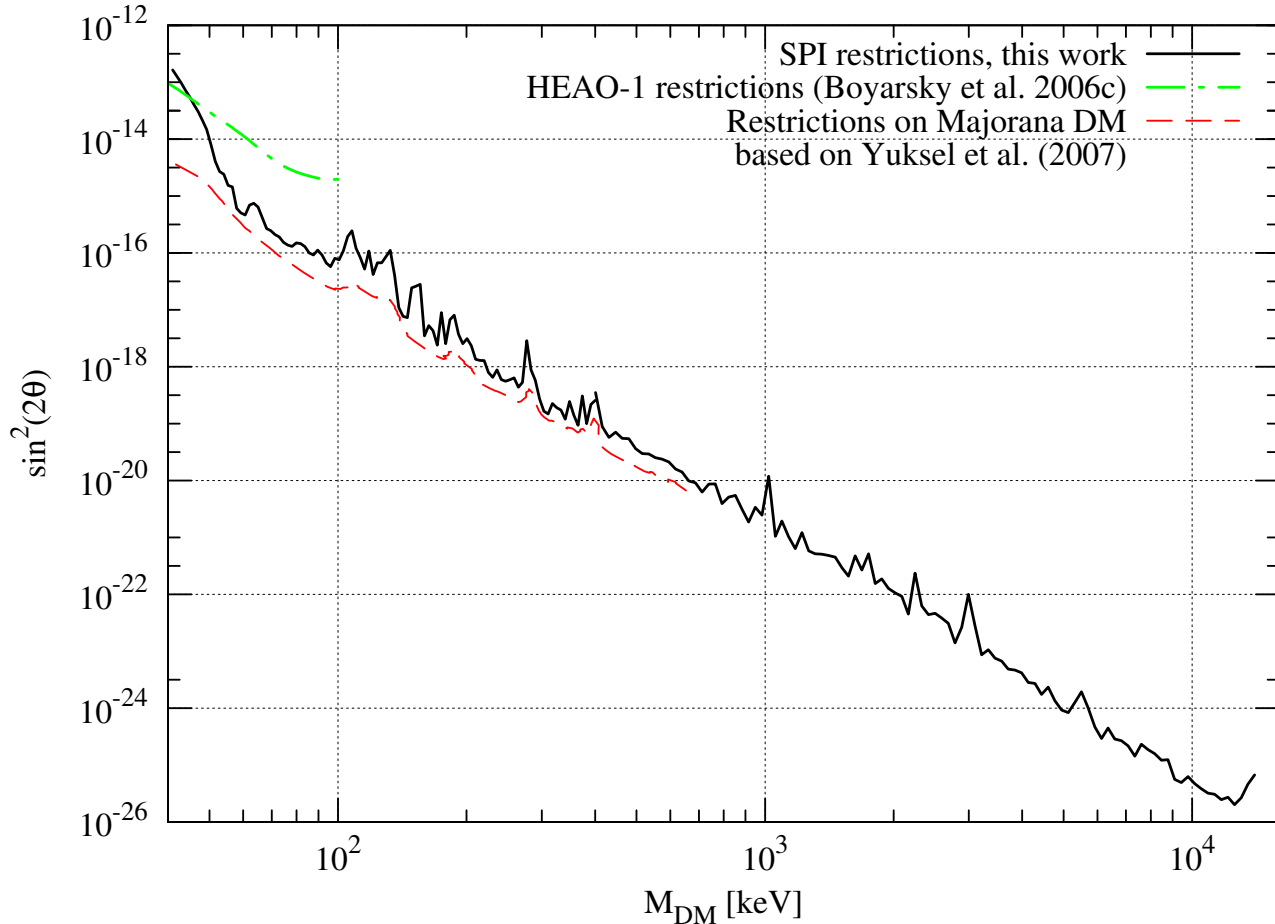


Figure 10. Upper bound on the mixing angle of the DM sterile neutrino as a function of the sterile neutrino mass, obtained from the analysis of the background spectrum of the pointings toward the inner 13° of the Galaxy. For masses ≤ 700 keV the restrictions from Yuksel et al. (2007) (divided by the factor 2, due to the Majorana nature of the DM) are also shown in dashed line (see Discussion). For masses < 100 keV previous restrictions from HEAO-1 (Boyarsky et al. 2006c) are also shown. The region *above* the curve is excluded.

40 keV – 700 keV. To facilitate the comparison, we plot the restrictions of Y07 on Fig. 10, (divided by the factor of 2 to translate them into the restrictions for the Majorana, rather than Dirac sterile neutrino DM, see footnote 6, p 5). As the data, used in our work, has about 5 times longer exposure than the *INTEGRAL* first years data, on which the results of Y07 are based, one could have expected a factor ≈ 2 stronger results in our case. However, the Fig. 10 shows the opposite. The reason for that is as follows. For the SPI the sensitivity towards the line search from a particular source depends on the shape of the source. In particular, the results of Teegarden & Watanabe (2006) (TW06), on which the work of Y07 was based, were obtained under the assumption of a particular diffuse source (10° Gaussian). As any realistic DM profile is much flatter than the 10° Gaussian, the results of TW06 cannot be applied directly for the case of the DM line search. They should be rescaled to account for the diffuse nature of the DM source (c.f. Section 5). Apart from that, the estimated DM signal from the inner part of the Galaxy is about 2 times stronger in Y07 than in our work. As the DM signal in the direction of the GC is the most uncertain one, we adopted the conservative flat profile everywhere inside the solar radius, to minimize this uncertainty.

Acknowledgements

We would like to thank B. Teegarden and K. Watanabe for useful discussion. D.M. is grateful to the Scientific and Educational Center¹² of the Bogolyubov Institute for Theoretical Physics in Kiev, Ukraine, and especially to V. Shadura, for creating wonderful atmosphere for young Ukrainian scientists, and to Ukrainian Virtual Roentgen and Gamma-Ray Observatory VIRGO.UA¹³ and computing cluster of Bogolyubov Institute for Theoretical Physics¹⁴, for using their computing resources. The work of D.M. was supported by the Swiss National Science Foundation and the Swiss Agency for Development and Cooperation in the framework of the programme SCOPES - Scientific co-operation between Eastern Europe and Switzerland. The work of A.B. was (partially) supported by the EU 6th Framework Marie Curie Research and Training network "UniverseNet" (MRTN-CT-2006-035863). O.R. would like to acknowledge support of the Swiss Science Foundation.

¹² <http://sec.bitp.kiev.ua>

¹³ <http://virgo.bitp.kiev.ua>

¹⁴ <http://grid.bitp.kiev.ua>

REFERENCES

- Abazajian, K. N., Markevitch, M., Koushiappas, S. M., & Hickox, R. C. 2007, *Phys. Rev. D*, 75, 063511, ADS, arXiv:astro-ph/0611144
- Alard, C. 1999, *A&A*, 343, 10, ADS, arXiv:astro-ph/9808092
- Alcock, C., et al. 2000, *ApJ*, 541, 270, ADS
- Allain, M., & Roques, J.-P. 2006, *A&A*, 447, 1175, ADS
- Asaka, T., Laine, M., & Shaposhnikov, M. 2007, *JHEP*, 01, 091, hep-ph/0612182
- Asaka, T., & Shaposhnikov, M. 2005, *Phys. Lett.*, B620, 17, hep-ph/0505013
- Attie, D. et al. 2003, *A&A*, 411, L71, ADS, arXiv:astro-ph/0308504
- Avila-Reese, V., Colín, P., Valenzuela, O., D'Onghia, E., & Firmani, C. 2001, *ApJ*, 559, 516, ADS, arXiv:astro-ph/0010525
- Bahcall, J. N., & Soneira, R. M. 1980, *ApJS*, 44, 73, ADS
- Baltz, E. A., & Murayama, H. 2003, *JHEP*, 5, 67, ADS, arXiv:astro-ph/0108172
- Barger, V. D., Phillips, R. J. N., & Sarkar, S. 1995, *Phys. Lett.*, B352, 365, hep-ph/9503295
- Battaglia, G., et al. 2005, *Mon. Not. Roy. Astron. Soc.*, 364, 433, astro-ph/0506102
- Beacom, J. F., & Yüksel, H. 2006, *Phys. Rev. Lett.*, 97, 071102, ADS, arXiv:astro-ph/0512411
- Bereziani, Z. G., & Khlopov, M. Y. 1990, *Sov. J. Nucl. Phys.*, 52, 60
- Bereziani, Z. G., Vysotsky, M. I., & Khlopov, M. Y. 1987, *Sov. J. Nucl. Phys.*, 45, 1065
- Bereziani, Z. G., Vysotsky, M. I., Yurov, V. P., Doroshkevich, A. G., & Khlopov, M. Y. 1990, *Sov. J. Nucl. Phys.*, 51, 1020
- Bergstrom, L. 2000, *Rept.Prog.Phys.*, 63, 793, hep-ph/0002126
- Bertone, G., Buchmuller, W., Covi, L., & Ibarra, A. 2007, arXiv:0709.2299 [astro-ph]
- Bertone, G., Hooper, D., & Silk, J. 2005, *Phys. Rept.*, 405, 279, hep-ph/0404175
- Bode, P., Ostriker, J. P., & Turok, N. 2001, *ApJ*, 556, 93, astro-ph/0010389
- Boehm, C., Hooper, D., Silk, J., Casse, M., & Paul, J. 2004, *Phys. Rev. Lett.*, 92, 101301, astro-ph/0309686
- Boehm, C., Orloff, J., & Salati, P. 2006, *Physics Letters B*, 641, 247, ADS, arXiv:astro-ph/0607437
- Bond, J. R., Efstathiou, G., & Silk, J. 1980, *Phys. Rev. Lett.*, 45, 1980, ADS
- Bond, J. R., Szalay, A. S., & Turner, M. S. 1982, *Phys. Rev. Lett.*, 48, 1636, ADS
- Boyarsky, A., den Herder, J. W., Neronov, A., & Ruchayskiy, O. 2007b, *Astropart. Phys.*, 28, 303, ADS, astro-ph/0612219
- Boyarsky, A., Iakubovskiy, D., Ruchayskiy, O., & Savchenko, V. 2007c, ADS, 0709.2301
- Boyarsky, A., Neronov, A., Ruchayskiy, O., & Shaposhnikov, M. 2006a, *MNRAS*, 370, 213, ADS, astro-ph/0512509
- . 2006b, *Phys. Rev. D*, 74, 103506, astro-ph/0603368
- Boyarsky, A., Neronov, A., Ruchayskiy, O., Shaposhnikov, M., & Tkachev, I. 2006c, *Phys. Rev. Lett.*, 97, 261302, astro-ph/0603660
- Boyarsky, A., Nevalainen, J., & Ruchayskiy, O. 2007a, *A&A*, 471, 51, ADS, astro-ph/0610961
- Boyarsky, A., Ruchayskiy, O., & Markevitch, M. 2006d, Submitted to *ApJ*, ADS, astro-ph/0611168
- Carr, J., Lamanna, G., & Lavalley, J. 2006, *Reports of Progress in Physics*, 69, 2475, ADS
- Cembranos, J. A. R., Feng, J. L., Rajaraman, A., Smith, B. T., & Takayama, F. 2006, ADS, hep-ph/0603067
- Cheng, L. X. et al. 1997, *ApJ*, 481, L43+, ADS
- Chung, D. J. H., Kolb, E. W., & Riotto, A. 1999, *Phys. Rev. D*, 59, 023501, hep-ph/9802238
- Crotty, P., Lesgourgues, J., & Pastor, S. 2004, *Phys. Rev.*, D69, 123007, hep-ph/0402049
- Dalcanton, J. J., & Hogan, C. J. 2001, *ApJ*, 561, 35, astro-ph/0004381
- Dar, A. 1995, *ApJ*, 449, 550, ADS, arXiv:astro-ph/9504082
- de Rujula, A., & Glashow, S. L. 1980, *Phys. Rev. Lett.*, 45, 942, ADS
- Diehl, R. et al. 2003, *A&A*, 411, L117, ADS
- Diemand, J., Kuhlen, M., & Madau, P. 2007, *ApJ*, 657, 262, ADS, astro-ph/0611370
- Dodelson, S., & Widrow, L. M. 1994, *Phys. Rev. Lett.*, 72, 17, hep-ph/9303287
- Doroshkevich, A. G., Khlopov, M. I., & Klypin, A. A. 1989, *MNRAS*, 239, 923, ADS
- Dubath, P. et al. 2005, *MNRAS*, 357, 420, ADS
- Dubovsky, S. L., Tinyakov, P. G., & Tkachev, I. I. 2005, *Phys. Rev. Lett.*, 94, 181102, ADS, arXiv:hep-th/0411158
- Fogli, G. L., Lisi, E., Marrone, A., Palazzo, A., & Rotunno, A. M. 2006, *Prog. Part. Nucl. Phys.*, 57, 71, ADS, arXiv:hep-ph/0506083
- Frère, J.-M., Ling, F.-S., Honorez, L. L., Nezri, E., Swillens, Q., & Vertongen, G. 2007, *Phys. Rev. D*, 75, 085017, ADS, arXiv:hep-ph/0610240
- Gilmore, G. 2007, ADS, astro-ph/0703370
- Gilmore, G., Wilkinson, M., Kleyna, J., Koch, A., Wyn Evans, N., Wyse, R. F. G., & Grebel, E. K. 2006, ADS, astro-ph/0608528
- Gilmore, G., Wilkinson, M. I., Wyse, R. F. G., Kleyna, J. T., Koch, A., Evans, N. W., & Grebel, E. K. 2007, *ApJ*, 663, 948, ADS, arXiv:astro-ph/0703308
- Gilmore, G., Wyse, R. F. G., & Kuijken, K. 1989, *ARA&A*, 27, 555, ADS
- Giunti, C. 2007, *Nucl. Phys. Proc. Suppl.*, 169, 309, hep-ph/0611125
- Goerdt, T., Moore, B., Read, J. I., Stadel, J., & Zemp, M. 2006, *MNRAS*, 368, 1073, ADS, astro-ph/0601404
- Gruber, D. E., Matteson, J. L., Peterson, L. E., & Jung, G. V. 1999, *ApJ*, 520, 124, astro-ph/9903492
- Hannestad, S., & Raffelt, G. 2004, *JCAP*, 0404, 008, hep-ph/0312154
- Hansen, S. H., Lesgourgues, J., Pastor, S., & Silk, J. 2002, *MNRAS*, 333, 544, astro-ph/0106108
- Hooper, D., Ferrer, F., Boehm, C., Silk, J., Paul, J., Evans, N. W., & Casse, M. 2004, *Phys. Rev. Lett.*, 93, 161302, ADS, arXiv:astro-ph/0311150
- Hui, L., Gnedin, N. Y., & Zhang, Y. 1997, *ApJ*, 486, 599, ADS, astro-ph/9608157
- Jean, P. et al. 2003, *A&A*, 411, L107, ADS
- Khlopov, M. Y. 1997, *Cosmoparticle Physics* (World Scientific Pub Co Inc)
- Klypin, A., Kravtsov, A. V., Valenzuela, O., & Prada, F. 1999, *ApJ*, 522, 82, ADS, arXiv:astro-ph/9901240
- Klypin, A., Zhao, H., & Somerville, R. S. 2002, *ApJ*, 573, 597, ADS, astro-ph/0110390
- Knödseder, J. et al. 2005, *A&A*, 441, 513, ADS, arXiv:astro-ph/0506026
- Koposov, S. et al. 2007, *ApJ*, 663, 948, ADS, 0706.2687
- Kravtsov, A. V., Klypin, A. A., Bullock, J. S., & Primack, J. R.

- 1998, *ApJ*, 502, 48, ADS, arXiv:astro-ph/9708176
- Kuijken, K., & Gilmore, G. 1989a, *MNRAS*, 239, 605, ADS
- . 1989b, *MNRAS*, 239, 651, ADS
- . 1989c, *MNRAS*, 239, 571, ADS
- . 1991, *ApJ*, 367, L9, ADS
- Kuzmin, V. A., & Tkachev, I. I. 1998, *JETP Lett.*, 68, 271, hep-ph/9802304
- . 1999, *Phys.Rept.*, 320, 199, hep-ph/9903542
- Lasserre, T., et al. 2000, *A&A*, 355, L39, ADS, arXiv:astro-ph/0002253
- McCammon, D. et al. 2002, *ApJ*, 576, 188, ADS, astro-ph/0205012
- Milne, A. P. et al. 1999, *Astr. Lett. Comm.*, 38, 441, ADS
- Moore, B. 1994, *Nature*, 370, 629, ADS
- Moore, B., Quinn, T., Governato, F., Stadel, J., & Lake, G. 1999, *MNRAS*, 310, 1147, ADS, astro-ph/9903164
- Navarro, J. F., Frenk, C. S., & White, S. D. M. 1997, *ApJ*, 490, 493, astro-ph/9611107
- Pagels, H., & Primack, J. R. 1982, *Phys. Rev. Lett.*, 48, 223, ADS
- Pal, P. B., & Wolfenstein, L. 1982, *Phys. Rev.*, D25, 766
- Palazzo, A., Cumberbatch, D., Slosar, A., & Silk, J. 2007, arXiv:0707.1495 [astro-ph]
- Penarrubia, J., McConnachie, A., & Navarro, J. F. 2007, ADS, astro-ph/0701780
- Picciotto, C., & Pospelov, M. 2005, *Physics Letters B*, 605, 15, ADS, arXiv:hep-ph/0402178
- Prantzos, N. 1993, *A&AS*, 97, 119, ADS
- Purcell, W. R. et al. 1997, *ApJ*, 491, 725, ADS
- Rasera, Y., Teyssier, R., Sizun, P., Cassé, M., Fayet, P., Cordier, B., & Paul, J. 2006, *Phys. Rev. D*, 73, 103518, ADS, arXiv:astro-ph/0507707
- Riemer-Sørensen, S., Hansen, S. H., & Pedersen, K. 2006, *ApJ*, 644, L33, ADS, astro-ph/0603661
- Ruchayskiy, O. 2007, in *Proceedings of the 11th Marcel Grossmann Meeting on General Relativity*, ed. H. Kleinert, R. Jantzen, & R. Ruffini (World Scientific), arXiv:0704.3215 [astro-ph]
- Sánchez-Conde, M. A., Prada, F., & Łokas, E. L. 2006, in *American Institute of Physics Conference Series*, 125–131, ADS
- Seljak, U., Makarov, A., McDonald, P., & Trac, H. 2006, *Phys. Rev. Lett.*, 97, 191303, astro-ph/0602430
- Shaposhnikov, M. 2007, in *Proceedings of the 11th Marcel Grossmann Meeting on General Relativity*, ed. H. Kleinert, R. Jantzen, & R. Ruffini (World Scientific), astro-ph/0703673
- Shaposhnikov, M., & Tkachev, I. 2006, *Phys. Lett.*, B639, 414, hep-ph/0604236
- Shi, X.-d., & Fuller, G. M. 1999, *Phys. Rev. Lett.*, 82, 2832, astro-ph/9810076
- Simon, J. D., & Geha, M. 2007, 706, ADS, 0706.0516
- Sizun, P., Cassé, M., & Schanne, S. 2006, *Phys. Rev. D*, 74, 06314, ADS, arXiv:astro-ph/0607374
- Skinner, G., & Connell, P. 2003, *A&A*, 411, L123, ADS, arXiv:astro-ph/0308444
- Spergel, D. N., et al. 2007, *Astrophys. J. Suppl.*, 170, 377, astro-ph/0603449
- Strumia, A., & Vissani, F. 2006, hep-ph/0606054
- Tasitsiomi, A., Gaskins, J., & Olinto, A. V. 2004, *Astropart. Phys.*, 21, 637, astro-ph/0307375
- Teegarden, B. J. et al. 2004, in *ESA Special Publication*, Vol. 552, 5th INTEGRAL Workshop on the INTEGRAL Universe, ed. V. Schoenfelder, G. Lichti, & C. Winkler, 819–, ADS
- Teegarden, B. J., & Watanabe, K. 2006, *ApJ*, 646, 965, ADS, arXiv:astro-ph/0604277
- Tremaine, S., & Gunn, J. E. 1979, *Phys. Rev. Lett.*, 42, 407
- Vedrenne, G. et al. 2003, *A&A*, 411, L63, ADS
- Viel, M., Becker, G. D., Bolton, J. S., Haehnelt, M. G., Rauch, M., & Sargent, W. L. W. 2007, 709, ADS, 0709.0131
- Viel, M., Lesgourgues, J., Haehnelt, M. G., Matarrese, S., & Riotto, A. 2005, *Phys. Rev.*, D71, 063534, ADS, astro-ph/0501562
- . 2006, *Phys. Rev. Lett.*, 97, 071301, astro-ph/0605706
- Watson, C. R., Beacom, J. F., Yuksel, H., & Walker, T. P. 2006, *Phys. Rev.*, D74, 033009, astro-ph/0605424
- Weidenspointner, G. et al. 2003, *A&A*, 411, L113, ADS
- . 2007, ADS, astro-ph/0702621
- . 2006, *A&A*, 450, 1013, ADS, arXiv:astro-ph/0601673
- Yuksel, H., Beacom, J. F., & Watson, C. R. 2007, 706, ADS, 0706.4084
- Zhang, L., Chen, X., Kamionkowski, M., Si, Z., & Zheng, Z. 2007, *Phys. Rev. D*, 76, 0613013(R), 0704.2444

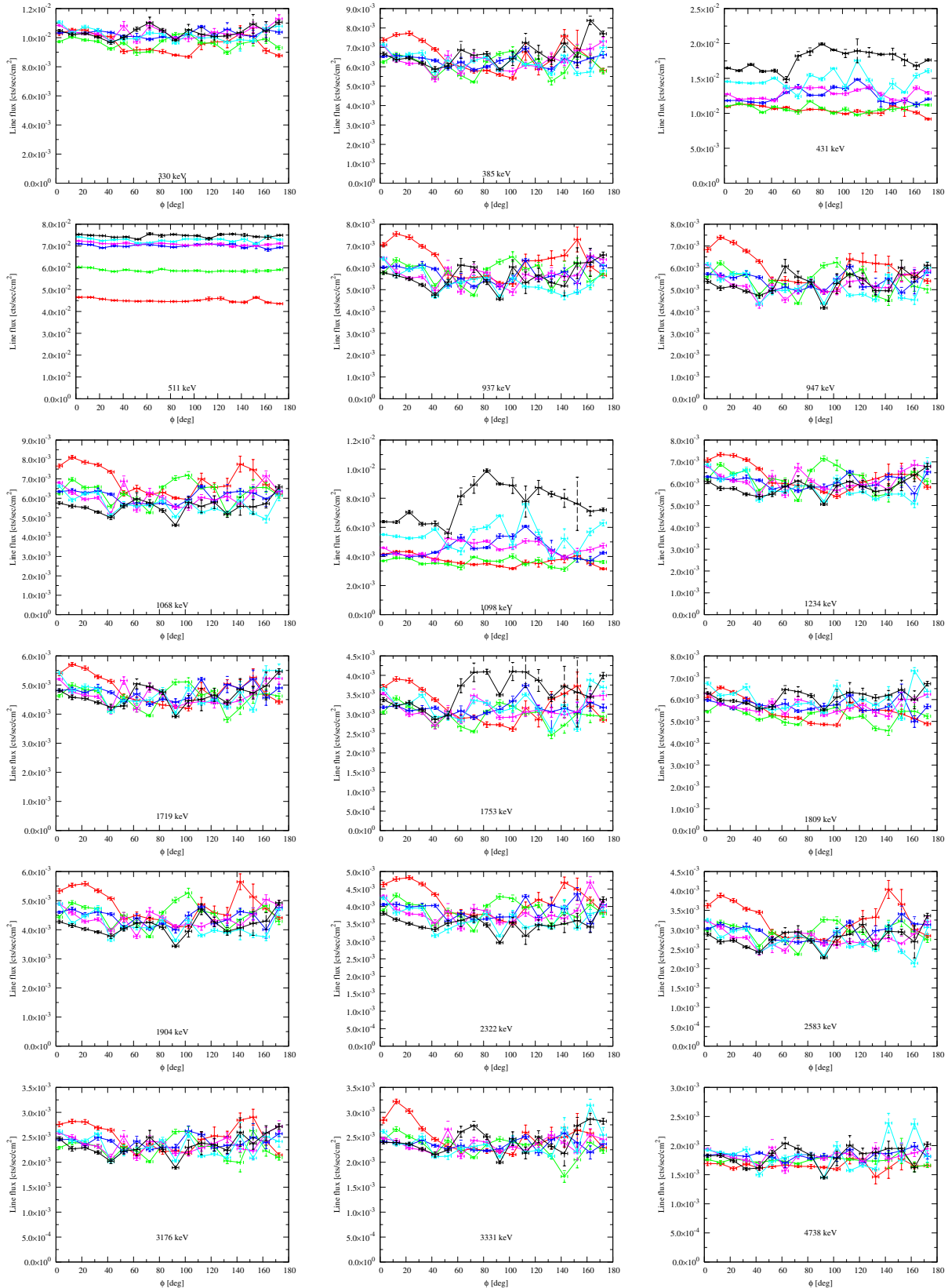


Figure 13. Line flux as a function of the off-GC angle ϕ for the ‘candidate’ lines from Table 3 (page 11). For all lines the flux does not depend on the off-GC angle (with 95 – 100% of all points lying within 3 standard deviations from the average). Different colors represent different phases (see Table 2, p. 9).

E [keV]	$\langle F \rangle$	σ_F	F_{\min}	F_{\max}	$\frac{F_{\max} - F_{\min}}{F_{\min}}$
330	9.6e-03	5.8e-04	8.7e-03	1.1e-02	0.23
	9.6e-03	4.0e-04	8.9e-03	1.0e-02	0.15
	1.0e-02	3.4e-04	9.3e-03	1.1e-02	0.16
	1.0e-02	5.2e-04	9.7e-03	1.2e-02	0.23
	1.0e-02	4.7e-04	9.6e-03	1.2e-02	0.24
	1.0e-02	6.1e-04	9.7e-03	1.3e-02	0.33
385	6.6e-03	7.3e-04	5.4e-03	8.0e-03	0.48
	6.1e-03	4.8e-04	5.2e-03	6.8e-03	0.31
	6.3e-03	3.9e-04	5.3e-03	7.1e-03	0.32
	6.2e-03	5.4e-04	5.2e-03	7.4e-03	0.42
	6.2e-03	5.0e-04	5.5e-03	7.6e-03	0.40
	6.7e-03	5.5e-04	5.8e-03	8.4e-03	0.44
431	1.1e-02	5.3e-04	9.2e-03	1.2e-02	0.26
	1.1e-02	5.7e-04	9.5e-03	1.2e-02	0.26
	1.2e-02	1.0e-03	1.0e-02	1.5e-02	0.43
	1.3e-02	8.1e-04	1.1e-02	1.4e-02	0.32
	1.4e-02	1.4e-03	1.2e-02	1.8e-02	0.45
	1.8e-02	1.5e-03	1.4e-02	2.0e-02	0.45
511	4.5e-02	7.8e-04	4.4e-02	4.7e-02	0.07
	5.9e-02	5.8e-04	5.8e-02	6.0e-02	0.04
	7.0e-02	8.5e-04	6.8e-02	7.2e-02	0.05
	7.1e-02	6.7e-04	6.9e-02	7.2e-02	0.04
	7.3e-02	8.7e-04	7.1e-02	7.4e-02	0.05
	7.5e-02	7.4e-04	7.3e-02	7.6e-02	0.03
937	6.3e-03	7.2e-04	5.2e-03	7.7e-03	0.47
	5.8e-03	5.4e-04	4.7e-03	6.6e-03	0.40
	5.7e-03	4.3e-04	4.9e-03	6.5e-03	0.33
	5.6e-03	5.4e-04	4.6e-03	6.6e-03	0.44
	5.3e-03	5.5e-04	4.7e-03	7.5e-03	0.60
	5.5e-03	5.0e-04	4.6e-03	6.6e-03	0.44
947	6.0e-03	7.2e-04	4.9e-03	7.4e-03	0.51
	5.4e-03	5.8e-04	4.4e-03	6.5e-03	0.49
	5.3e-03	4.4e-04	4.4e-03	6.1e-03	0.40
	5.2e-03	5.0e-04	4.3e-03	6.1e-03	0.43
	5.0e-03	6.0e-04	4.3e-03	7.0e-03	0.61
	5.3e-03	5.2e-04	4.2e-03	6.5e-03	0.55
1068	6.9e-03	7.2e-04	5.8e-03	8.2e-03	0.40
	6.3e-03	5.5e-04	5.2e-03	7.3e-03	0.41
	6.1e-03	4.2e-04	5.3e-03	7.0e-03	0.33
	6.0e-03	5.3e-04	5.1e-03	7.2e-03	0.41
	5.6e-03	4.5e-04	4.9e-03	6.8e-03	0.38
	5.5e-03	4.1e-04	4.6e-03	6.6e-03	0.43
1098	3.7e-03	3.9e-04	3.1e-03	4.6e-03	0.49
	3.7e-03	2.5e-04	3.1e-03	4.0e-03	0.30
	4.5e-03	6.6e-04	3.1e-03	6.1e-03	0.95
	4.5e-03	4.8e-04	3.6e-03	5.5e-03	0.56
	5.4e-03	1.0e-03	3.8e-03	7.6e-03	0.99
	7.6e-03	1.3e-03	5.1e-03	9.9e-03	0.94
1234	6.4e-03	5.9e-04	5.4e-03	7.4e-03	0.36
	6.2e-03	5.4e-04	5.2e-03	7.2e-03	0.38
	6.0e-03	3.7e-04	5.2e-03	6.6e-03	0.27
	6.1e-03	4.6e-04	5.4e-03	6.9e-03	0.27
	5.8e-03	5.5e-04	5.1e-03	7.6e-03	0.50
	5.8e-03	4.0e-04	5.0e-03	6.8e-03	0.35
1719	4.9e-03	5.0e-04	4.0e-03	5.7e-03	0.42
	4.6e-03	3.8e-04	3.8e-03	5.1e-03	0.35
	4.7e-03	3.1e-04	3.9e-03	5.2e-03	0.34
	4.6e-03	3.8e-04	4.1e-03	5.4e-03	0.32
	4.5e-03	4.0e-04	3.9e-03	5.5e-03	0.40
	4.7e-03	4.2e-04	3.9e-03	5.7e-03	0.46
1753	3.2e-03	4.1e-04	2.6e-03	4.0e-03	0.53
	3.0e-03	2.7e-04	2.4e-03	3.4e-03	0.41
	3.1e-03	2.7e-04	2.4e-03	3.7e-03	0.59
	3.1e-03	3.0e-04	2.6e-03	3.7e-03	0.43
	3.1e-03	3.5e-04	2.6e-03	3.9e-03	0.51
	3.6e-03	4.5e-04	2.7e-03	4.3e-03	0.61
1809	5.5e-03	5.1e-04	4.6e-03	6.6e-03	0.43
	5.2e-03	3.3e-04	4.6e-03	5.8e-03	0.28
	5.7e-03	3.3e-04	5.0e-03	6.3e-03	0.27
	5.7e-03	3.5e-04	5.2e-03	6.5e-03	0.24
	5.9e-03	4.7e-04	5.0e-03	7.3e-03	0.46
	6.1e-03	3.9e-04	5.4e-03	7.0e-03	0.30
1904	4.8e-03	5.1e-04	4.1e-03	5.6e-03	0.39
	4.5e-03	3.9e-04	3.8e-03	5.3e-03	0.40
	4.4e-03	3.2e-04	3.7e-03	5.2e-03	0.39
	4.3e-03	4.0e-04	3.6e-03	5.2e-03	0.44
	4.1e-03	3.7e-04	3.6e-03	5.2e-03	0.42
	4.1e-03	3.3e-04	3.4e-03	4.9e-03	0.43
2322	4.2e-03	4.0e-04	3.5e-03	4.9e-03	0.39
	3.9e-03	3.0e-04	3.2e-03	4.3e-03	0.34
	3.9e-03	2.9e-04	3.3e-03	4.7e-03	0.42
	3.8e-03	3.2e-04	3.3e-03	4.7e-03	0.43
	3.6e-03	2.9e-04	3.1e-03	4.2e-03	0.35
	3.5e-03	2.8e-04	3.0e-03	4.2e-03	0.42
2583	3.2e-03	4.1e-04	2.6e-03	4.0e-03	0.53
	2.9e-03	2.6e-04	2.4e-03	3.3e-03	0.41
	2.9e-03	2.2e-04	2.4e-03	3.4e-03	0.42
	2.8e-03	2.6e-04	2.4e-03	3.4e-03	0.44
	2.7e-03	2.6e-04	2.1e-03	3.3e-03	0.52
	2.8e-03	2.6e-04	2.3e-03	3.4e-03	0.48
3176	2.5e-03	2.5e-04	2.1e-03	3.0e-03	0.41
	2.3e-03	1.9e-04	1.9e-03	2.7e-03	0.40
	2.4e-03	1.6e-04	1.9e-03	2.7e-03	0.41
	2.4e-03	1.9e-04	2.0e-03	2.7e-03	0.36
	2.3e-03	2.1e-04	1.9e-03	2.7e-03	0.42
	2.3e-03	2.2e-04	1.9e-03	2.9e-03	0.54
3331	2.5e-03	2.9e-04	2.2e-03	3.2e-03	0.50
	2.3e-03	2.0e-04	1.7e-03	2.7e-03	0.55
	2.4e-03	1.5e-04	2.0e-03	2.8e-03	0.35
	2.3e-03	1.7e-04	2.0e-03	2.7e-03	0.33
	2.3e-03	2.1e-04	2.1e-03	3.1e-03	0.51
	2.4e-03	2.3e-04	2.0e-03	2.9e-03	0.44
4738	1.7e-03	6.2e-05	1.5e-03	1.8e-03	0.22
	1.7e-03	6.5e-05	1.5e-03	1.9e-03	0.24
	1.8e-03	9.9e-05	1.5e-03	2.0e-03	0.31
	1.8e-03	1.3e-04	1.5e-03	2.0e-03	0.38
	1.8e-03	2.1e-04	1.5e-03	2.4e-03	0.64
	1.8e-03	1.7e-04	1.4e-03	2.1e-03	0.46
5186	1.5e-03	6.7e-05	1.4e-03	1.7e-03	0.26
	1.6e-03	5.5e-05	1.5e-03	1.8e-03	0.16
	1.8e-03	9.4e-05	1.6e-03	2.1e-03	0.35
	1.8e-03	6.4e-05	1.6e-03	2.0e-03	0.24
	1.8e-03	6.9e-05	1.6e-03	1.9e-03	0.18
	1.8e-03	1.2e-04	1.5e-03	2.0e-03	0.32
5208	1.5e-03	8.8e-05	1.2e-03	1.8e-03	0.51
	1.6e-03	5.6e-05	1.5e-03	1.8e-03	0.21
	1.7e-03	5.8e-05	1.6e-03	1.9e-03	0.16
	1.7e-03	5.3e-05	1.6e-03	1.9e-03	0.15
	1.8e-03	8.0e-05	1.6e-03	2.1e-03	0.28
	1.8e-03	1.3e-04	1.5e-03	2.1e-03	0.39

Table 4. Characteristics of the spatial profiles of the candidate lines from Table 3. For each line (and for each of 6 phases) we compute the average $\langle F \rangle$, the standard deviation (average scatter of the points around its mean value) σ_F , minimal and maximal values and the ratio of $(F_{\max} - F_{\min})/F_{\min}$, which gives the *upper* bound on the share of DM, present in the given line.